HER⬤N

vol. 37
1992
no. 3

Contents

NUMERICAL SIMULATION OF HYDRATION AND MICROSTRUCTURAL DEVELOPMENT IN HARDENING CEMENT-BASED MATERIALS

K. van Breugel

Delft University of Technology,
Department of Civil Engineering,
Division of Mechanics and Structures/Concrete Structures

Publication in HERON since 1970

Numerical Simulation of Hydration and Microstructural Development in Hardening Cement-Based Materials

1 Introduction

1.1 *General Scope of the Project*

Quality control on the building site is one of the major challenges in engineering practice today. Both *durability* and *functionality* must be envisaged in this respect. A reduction of the durability is to be expected when early-age temperature-induced microcracking occurs due to different coefficients of thermal expansion of matrix and aggregates. Reduced functionality may occur when thermal stresses give rise to through-cracks causing leakage in liquid retaining structures, cellars, etc. (Fig. 1.1). In order to enhance the quality and performance of concrete structures, control of temperatures and associated thermal stresses must, therefore, be given due attention. For quantification of the effectiveness of technological and technical measures for improving the quality of the product, i.e. to reduce thermal stresses and the probability of cracking, numerical simulations are becoming increasingly important.

Most of the programs for temperature predictions operational in engineering practice are based the differential equation of Fourier. The input for most of these "macro-level programs" consists of, among other things, either an adiabatic, an isothermal or a semi-adiabatic hydration curve of the mix in view. In the mathematical calculation algorithms these input curves are to be adjusted for the actual temperature at which hydration occurs. The output consists of the actual reaction temperature and the rate of heat liberation. The degree of heat liberation is often considered identical with the degree of hydration.

The latter quantity is a major parameter which determines the physical properties of the paste or concrete, like porosity, strength and modulus of elasticity. More recently
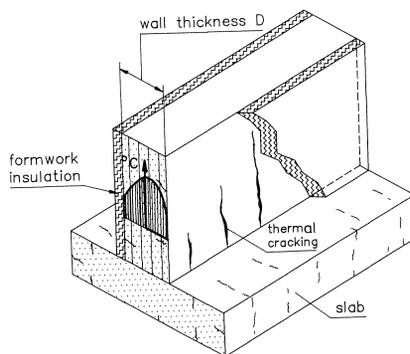
Fig. 1.1   Early-age thermal cracking in a slab-wall construction. Through-cracks and surface cracks [4].

3

also the early-age time-dependent properties like creep and relaxation have been considered in the light of changes in the degree of hydration, i.e. as a function of microstructural development [1, 2, 3]. The role of the degree of hydration in both temperature, strength and stress calculations makes this quantity to a key-parameter in the thermal analysis of hardening concrete. This implies that the accuracy and reliability of early-age thermal analysis strongly depends on the accuracy with which the degree of hydration is determined.

The importance of accurate predictions of the degree of hydration compels to detailed investigations of all mechanisms and processes involved in hydration and microstructural development. With these investigations we enter a very complex field in which *chemical, stereological, physical, colloidal* and *crystallographic* aspects are involved. The complexity of this multi-aspect problem is a challenge for the modern *Computational Materials Science.* It is particularly in this field that mutually interfering mechanisms and processes operational in hydration and microstructural development can be modelled and simulated in a way that far exceeds classic analytical procedures. Aware of inevitable restrictions of even the most sophisticated computer programs, it seems to the author that with numerical simulation programs we now have, more than ever before, the possibility to benefit from the huge amounts of information about hydration and microstructure brought together by different disciplines and to make all this information accessible for and operational in engineering practice.

1.2   *Objectives of the Study*

In Section 1.1 it has been emphasized that for both temperature and strength calculations, as well as for the prediction of stresses and the risk of cracking, the degree of hydration is a most important factor. The accuracy and reliability of macro-level models for temperature, strength and stress calculations, therefore, largely depend on the accuracy with which the degree of hydration can be determined. Besides inaccuracies in the calculated degree of hydration, strength and stress predictions also suffer from a lack of fundamental knowledge with respect to the *correlation* between the degree of hydration and associated microstructural formation on the one hand, and strength and stress development on the other.

The complexity of the correlation between microstructural development and the development of material properties, as well as the need for further research on this topic, has been emphasized by many authors (for a survey, see [4]). A *lack of fundamental rigour* in defining the relevant characteristics of the starting materials and of the hydration products *rather than a lack of information about individual processes and mechanisms* is a major reason why adequate models for predicting the progress of the hydration process and structural development are still missing. This lack of rigour causes a kind of status quo as far as mathematical modelling of hydration processes and structural formation is concerned. This status quo, in turn, means that a lot of the most interesting information as regards micro[1] and meso[2] level research is not transferred to the macro[3] or engineering level.

[1,2,3] In this report the definitions for micro-, meso- and macro-level are according to Wittmann [5].

The present study must be regarded as an attempt to bridge the gap between aforementioned research levels. For this purpose a computer-based simulation model has been developed called HYMOSTRUC, the acronym for HYDRATION, MORPHOLOGY and STRUCTURAL development. The aims of the research project and of the simulation model in particular are the following.

1. *Development of a simulation model with which adiabatic and/or isothermal hydration curves of Portland cement-based materials can be predicted. These curves could serve as input for numerical evaluation of thermal effects in hardening concrete structures.*
2. *The simulation model should take into consideration mutual interferences between the hydration process and the development of microstructure. Morphological features, particularly temperature-related ones, should be dealt with.*
3. *The correlation between structural development (as it will be considered in the model) and the development of material properties shall be evaluated.*
4. *In view of the desired applicability of the results in engineering practice indications shall be given as regards the reliability and accuracy of the predictions.*

In order to enhance the applicability in engineering practice the simulation model should preferrably be developed for a Personal Computer environment. In order to be able to implement additional options in the model in later stages without drastic restructuring of the model, the structure of the model should be as "open" as possible (see also Jennings [6] and [4]).

2 Aspects of Hydration and Microstructural Development

2.1 *General*

For a correct interpretation of hydration data, as well as for consistent modelling of the hardening process in a poly-mineral and poly-size water-cement system, one should have a complete picture of all parameters which affect hydration and microstructural development. This means that *chemical, physical, stereological* and *granular* aspects have to be considered. For a more complete survey of these aspects reference is made to [4]. In this chapter some of the most important results of this survey are summarized. Thereby we restrict ourself to those results which are relevant in view of the interpretation of hydration data, for judgment of microstructural aspects and which may be helpful when defining the basic assumptions which constitute the framework within which the simulation model will be developed.

2.2 *Chemical and Granular Characteristic of Cement*

Chemical Composition of Portland Cement
One of the input parameters of numerical models is the clinker composition of the cement. This clinker composition is a function of the mineral composition of the raw materials. Small deviations in the mineral composition influence the clinker composi-

tion significantly. Mathematical models for calculating the clinker composition on the basis of the mineral composition exhibit a wide scatter [4]. The often applied Bogue-method *underestimates* the amount of C_3S and *overestimates* the C_2S content.

The clinker composition appears to be a function of the particle size. The difference between the C_3S content of small and large particles can reach up to 10...20%. Differences in the C_2S content of small and large particles of the same order of magnitude have been reported. Differences of this order of magnitude may affect the rate of hydration in different stages of the hydration process substantially.

Particle Shape and Specific Surface

From both a theoretical point of view and microscopic observations it is evident that cement particles are not spherical. This is further confirmed by adsorption measurements of the specific surfaces of cement. Adsorption data show the "actual" surface areas to be 2 to 3 times the Blaine surfaces. Actual particle shapes significantly deviating from a spherical shape can have significant consequences for the interpretation of hydration data. Misinterpretations with respect to hydration depths, the thickness of the layer of hydration products, hydration mechanisms and diffusion coefficients have to be expected.

Particle Size Distribution

The actual particle size distribution of cement generally exhibits distinct discontinuities. As long as mathematical functions for the cumulative weight distribution of cement do not account for these discontinuities, it is questionable whether it would be worthwhile to try to achieve a very high correlation of these functions with the actual cumulative weight distributions. The Rosin-Rammler function, although probably less accurate in the fine particle range than other function, is, therefore, considered to be accurate enough for the mathematical description of the particle size distribution and will be used in this study.

2.3   *Hydration of Cement-Based Materials*

2.3.1   Hydration Mechanisms

Hydration mechanisms of Portland cement have been investigated for the past hundred years or so, but are still not clearly understood [7]. Basically two different schools can be distinguished, one supporting the *topochemical concept* and the other the *through-solution concept*.

Topochemical and Through-Solution Mechanisms

The debate on whether cement hydration proceeds *topochemically (Fig. 2.1a)* or according to a *through-solution mechanism (Fig. 2.1b)* dates back to the very beginning of cement chemistry. The subject is of great importance in view of mathematical modelling of both the hydration process and microstructural development.

6

a. Topochemical reaction   b. Through-solution mechanism
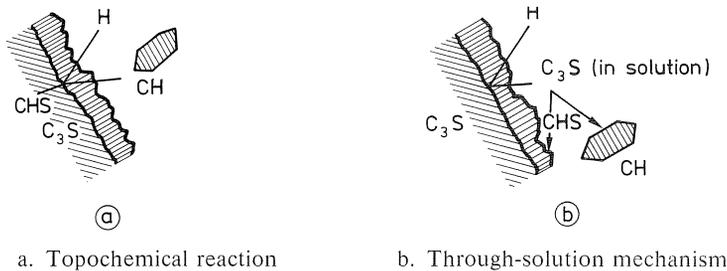
Fig. 2.1   Schematic representation of proposed hydration mechanisms (after [9]).

The topochemical concept was launched by Michaelis [8] at the beginning of this century.

Immediately after the first contact of the cement with water a calcium-rich silicious clinker would liberate Ca^{++} ions into the solution. A calcium-poor skeleton is left which reacts with the calcium-rich solution. This is accompanied by swelling of the hydration products compared with the original volume of the anhydrous cement.

The through-solution concept was first formulated by Le Chatelier [10] for plaster and Portland cement in the first decade of this century. In this concept dissolution of the anhydrous grain after contact of the cement with water is considered to be followed by hydration in the solution. The hydration products then precipitate on the grain surface.

Simultaneously Operating Mechanisms

Shebl et al. [11] explains that hydration of C_3S involves both through-solution reactions and topochemical reactions (solid-state reaction). The water/solid ratio would be an important factor in this respect. For low water/solid ratios the reaction would be predominantly topochemical, whereas for high water/solid ratios the through-solution mechanism would be more important. Both reactions could occur simultaneously.

The concept of simultaneously operating mechanisms is plausible indeed if the *outer products,* i.e. the products which are formed *outside* the original grain boundaries in a relatively water-rich environment, are formed by a through-solution mechanism, while the *inner products,* formed *inside* the original grain boundaries, are formed topochemically [12, 13].

2.3.2   Clinker Hydration versus Hydration of Individual Compounds

Rate of Reaction of Individual Constituents

The rates of reaction of individual constituents differ quite significantly. For C_3S and C_2S the rates of hydration are shown in Fig. 2.2 (from Lea [14]). Although there is, for several reasons, a substantial scatter in these hydration curves, there nevertheless remains a quite distinct difference between the rates of hydration of the individual compounds. Similar conclusions also hold for the hydration of C_3A and C_4AF.

It is to be expected that the rate of hydration of cement will somehow be a function of

7

a. C₃S-hydration
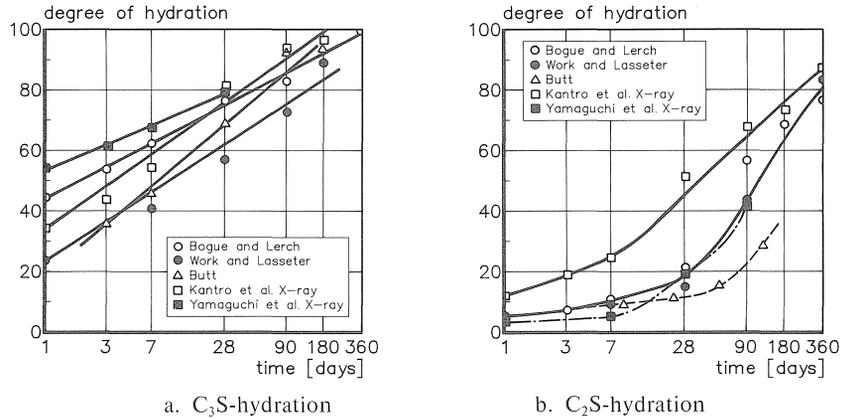
b. C₂S-hydration

Fig. 2.2   Rate of hydration of different pastes according to several authors (from [14]).

the rates of reaction of the individual constituent phases. Mathematical modelling of the interaction in a hydrating poly-mineral systems is very complicated. For that reason models developed in the past generally focus on only one of the two extreme concepts, i.e. the *Independent Hydration Concept* or the *Equal Fractional Rates Concept*.

Independent Hydration Concept
In the Independent Hydration Concept, schematically shown in Fig. 2.3a, any inter-action between hydrating constituents is disregarded. Non-uniformity of the rate of reaction of poly-mineral particles as observed by several authors might be interpreted as an argument in favour of the Independent Hydration Concept [15, 16, 17].

Independent Hydration

Equal Fractional Rates
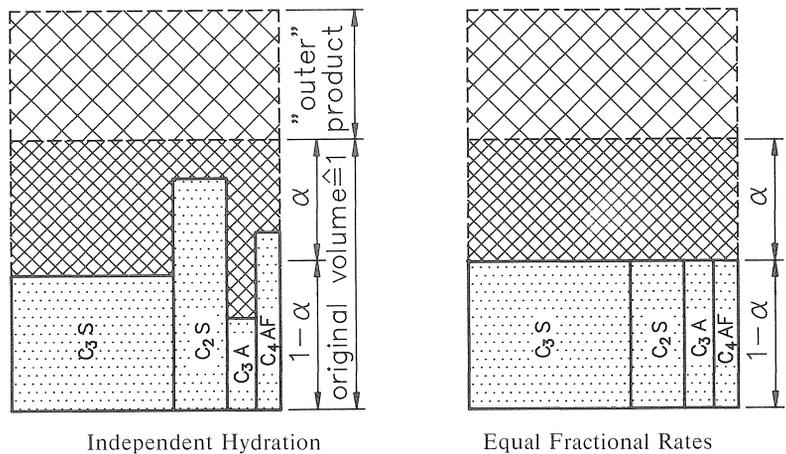
Fig. 2.3   Schematic representation of Independent Hydration Concept and hydration at Equal Fractional Rates ($\alpha =$ overall degree of hydration).

8

Equal Fractional Rates (EFR-concept)

From microscopic observations Brownmiller [18] concluded to the evidence of a gradual, uniform reduction of the particle size as hydration proceeds (see Fig. 2.3b). Any channelling of water into the grains to hydrate the more reactive constituents was not noticed. In a discussion with Brownmiller, Rexford [19] stated that hydration would indeed take place at a comparatively uniform overall rate which affected all of the cement compounds of a cement particle more or less simultaneously.

Hydration Mechanisms. Discussion

Experimental work of, among others, Bentur et al. [20], Yamaguchi [21] and Lehmann [22] indicates that in a polymineral system hydration of individual constituents proceeds *neither* at equal fractional rates *nor* independently from each other. Apart from interactions of a purely *chemical* nature at least two sources of *physical* interaction appear to exist, viz.:

1. *Changes in the effective constituent/water ratio, caused by differences in the rate of hydration of the individual constituents;*
2. *Diffusion processes, which would be responsible for a more equal rate of hydration of the individual constituents at later – diffusion-controlled – stages of the hydration process.*

The evidence of interactions make us reluctant to adopt the Independent Hydration Concept. At any rate this concept requires corrections for the existence of interactions in order to avoid misinterpretations of experimentally and theoretically obtained hydration data. Attempts to model the interactions between hydrating constituents, however, will soon lead to great difficulties. This subject has been discussed by many authors, but at present no universally accepted model is available that comprehensively and consistently describes how individual compounds interfere. The role of gypsum and alkalies in the hydration process further enhances the complexity of the subject. One step in view of "reconciliation" that what is in essence irreconcilable exists in the recognition that the degree of hydration is an *apparent, overall* or *global* value, representing a certain *average* of the degrees of hydration of the individual constituents. This, however, is no more than a first step and in fact no more than a matter of wording without doing anything to obviate the complications encountered in modelling. Another possibility in view of reconciliation would exist in defining the *rate of penetration of a uniform reaction front in a cement particle as a function of the chemical composition of the cement* [4]. Such a concept has been adhered when developing the simulation model as presented in Chapter 3.

2.4 *State of Water*

Since hardening of a cement paste is the result of the reaction between cement and water, it is to be expected that the state of water in the paste is an important factor in the rate of reaction. In a hydrating water-cement system the water is present in *roughly*

three different forms, viz. *chemically bound water, physically bound water* and *free* or *capillary water.*

Chemically Bound water

At complete hydration of cement, an amount of water of about 22%...25% of the weight of the anhydrous cement is chemically bound to the cement [23, 24]. In this form, which actually includes water molecules which are most tightly adhered to the surfaces of reaction products, it is considered to be an inherent part of the solid matter. The resulting volume of the reaction products is less than that of the added volumes of the constituents. Related to the original volume of the chemically bound water a volume reduction of about 18% to 26% is observed [25, 24].

Physically Bound water

As can be deduced already from Fig. 2.4 the amount of physically bound or adsorbed water actually depends on the relative humidity in the pore system. As a rough guide value for the amount of physically bound water a value of 15% of the weight of the anhydrous cement is generally adopted [23,24]. Together with the amount of chemically bound water, i.e. about 25% of the weight of the anhydrous cement the amount of water required for complete hydration would be about 40% of the weight of the cement.
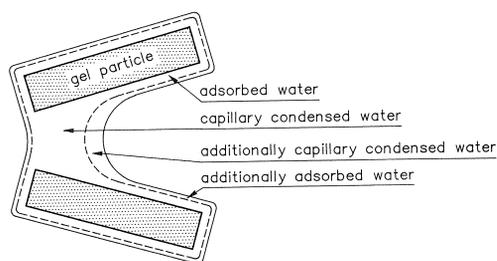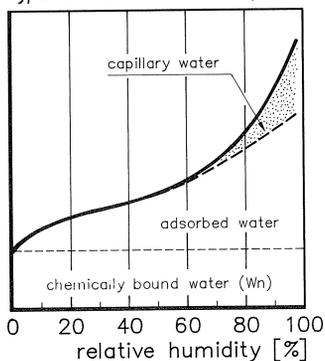
Fig. 2.4 Distribution of water in cement paste as a function of the relative humidity.
a. Diagrammatical representation of types of water in cement paste
b. Representation of adsorption isotherm including capillary condensation (after [26])

An adsorbed water layer with a thickness of 8 to 9 Å, i.e. the adsorption layer that remains at a relative humidity of about 80%, is thick enough to fill the gel pores with a diameter of about 20 Å almost completely with water. Assuming the 20 Å pores to be characteristic for the gel, it can be concluded that under normal curing conditions the gel is completely saturated. This part of the physically bound water is, therefore, considered to be part of the gel and is not available for further hydration.

10

Free Water

Water that is removed by heating of cement paste up to 105 °C is generally identified as free water. Water molecules of this free water are considered to behave like in bulk water.

Free water is often equalized with evaporable water. This water is assumed to be available for further hydration of the cement. Similar to what has been observed with respect to the borderline between chemically and physically bound water, the borderline between evaporable and non-evaporable water is not a very distinct one either [27]. Part of the evaporable water (which includes the physically bound water [24]) has been found to behave as a structural component of some hydrates, viz. the innermost adsorbed water layers.

2.5 *Microstructural Development*

2.5.1 Formation of Basic Skeleton

A schematic representation of the formation of structure as proposed by Locher et al. [28] is shown in Fig. 2.5. Reaction products formed at the surface of cement particles in the early stage of hydration generally consist of very small needles (ettringite) of 0.25 by 0.05 μm.

plastic phase   setting stage   basic skeleton   "stable" skeleton

a   b   c   d
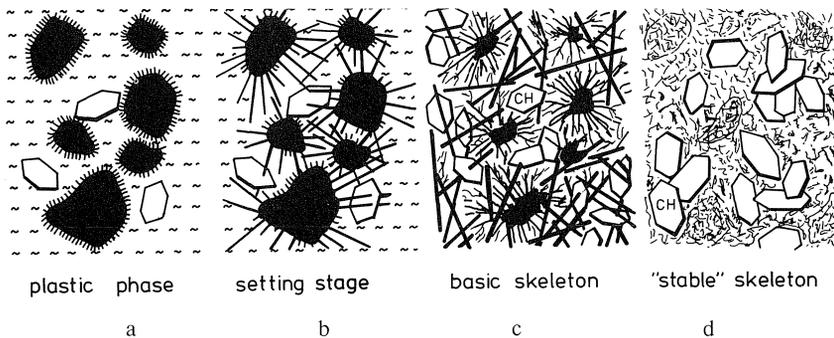
Fig. 2.5   Formation of reaction products and build-up of structure (after [28]).

After one hour of hydration these needles have developed to a size of 1 by 0.1 μm [29]. In subsequent stages of the hydration process ettringite needles may continue to grow and reach a length of 2 to 3 μm [30] and even up to 10 μm [31]. While growing they gradually bridge the interparticle distances of about 1 to 2 μm, forming a spatial network (Fig. 2.5b). With the formation of this network the position of the cement particles in the cement/water system is established.

In the early stage of the hydration process the formation of clusters of needle-like particles has been observed [32]. Probably the rapid dissolution of small particles – particles up to about 2 μm – allow for this clustering to a great extent. As the hydration process progresses these clusters interlock and grow together. Meanwhile CSH particles are formed radiating out from active centres into the water filled pores,

11

building up an increasingly dense, three-dimensional network [34, 33]. The characteristic fibril size of the CSHs in this stage of the reaction process is about 1 μm in length with a diameter of 0.01 μm. Plate-shaped CSH particles would have sizes of the same order of magnitude [35]. CH crystals are formed mainly in empty spaces and can develop into very large particles which envelop the hydrating cement particles [12].

The basic skeleton is formed between 7 and 28 days (Fig. 2.5c). As the hydration process further progresses the reaction products hardly grow in size, but new particles are formed, similar in size to those formed earlier [25, 24]. These new products settle in the empty space within the spatial network originally built up by the ettringite needles [36] (Fig. 2.5d).

2.5.2 Inner and Outer Product

Products formed outside the original grain boundaries are termed *outer product,* whereas reaction products formed inside these boundaries are called *inner product.* The density of outer product is generally considered to be less than that of inner product. This difference holds particularly in the early phase of hydration. During the hydration process this difference gradually vanishes due to volume constraints and associated merging of the outer product of expanding particles [37, 38]. This merging effect might be the reason why a distinct boundary between inner and outer product is not always observed [39, 40].

According to Daimon [41] the transformation of anhydrous C_3S grains into CSH gel occurs without a change in the shape of the grain. Preservation of the particle shape has also been observed in the case of hydrating cement particles [39]. Particle shape preservation does not hold for particles smaller than about 3 μm. These particles completely dissolve [43, 42] and only form an outer product which precipitates at the surface of large particles [33].

2.6 *Temperature Effects on Microstructure and Strength*

In line with numerous reports Odler et al. [44] found that curing at temperatures above 50 °C results in a lower ultimate strength. For an explanation of this phenomenon Kjellsen [45] refers to earlier work by Verbeck et al. [46], who suggested that in the case of curing at high temperatures the hydration products would be formed more immediately surrounding the hydrating cement particles, resulting in a denser gel. This would have two effects, viz. a *geometrical* and a *physical* effect. Firstly, a less expanded gel volume will generate fewer contact points and smaller contact surfaces between hydrating particles. Secondly, the denser gel might result in a decrease of the rate of hydration due to lower diffusion rates of ions to and from the surface of the anhydrous cement core into the solution. Particularly the first mentioned effect can be interpreted as being in full agreement with Bentur's observation that hydration at higher temperatures causes an increase of the capillary porosity of the paste [20], as well as with later work of Kjellsen et al. [47, 48].

12

Note that in the foregoing explanations the effect of temperature on strength development has been reduced to a geometrical, i.e. a *stereological problem,* viz. a mechanism of reduced expansion, and hence a reduced interference between hydrating particles. This geometry-oriented explanation offers interesting possibilities for mathematical modelling of the temperature effect on strength development.

2.7 *Microstructure and Strength Development. Summary and Discussion*

Strength development is closely linked to structural formation. Thereby it appears relevant to distinguish between the structural formation as it occurs in a neat cement paste (bulk hydration) and in the close vicinity of the matrix-aggregate interface (interface hydration).

"Interparticle" Structural Formation
Immediately after the first contact with water, cement particles start to dissolve and form reaction products. Hydrating particles of some size, from about 3 μm onwards, can be considered as expanding centres, generally assumed to be spheres. Within the original grain boundaries inner product is formed, whereas outside these boundaries the outer product is formed. Cement particles smaller than 3 μm are considered to form only outer products. The reaction products produced by these small particles will precipitate and merge with the outer product of larger particles, thus allowing for extra expansion to the latter particles. As long as particles do not make contact, their mode of expansion appears to be concentric-wise. This lends support to the idea that the outer product has a more or less constant morphological structure, i.e. constant porosity and density, albeit not unconditionally identical to the morphology and density of the inner product. As soon as expanding particles make contact, merging of outer products takes place under conditions of increasing volume constraint which can be expected to lead to local densification of the gel. As the hydration process progresses the number of contact points will increase. At the same time the earlier formed contact points will change into contact areas. Densification of outer product of expanding particles and embedding of smaller particles in the outer shell of the large particles, i.e. increasingly intensive merging of reaction products, is most probably the reason, at least in part, why in later stages of the hydration process a distinct difference in chemical composition and density of inner and outer product gradually vanishes.

Paste Strength
Strength is developed due to the increasing number of contact points and the increasing magnitude of the contact surface area between hydrating particles during the hydration process. Thinking in a scenario of expanding and merging particles implies that strength development has a distinct *stereological aspect.* The effect of the *w/c ratio* on strength development can easily be explained from a stereological point of view and is almost trivial. Moreover, there is also room to expect that *temperature effects* on strength development can be explained in stereological and geometrical terms, at least in part (Section 2.6).

13

The effect of the *chemical composition of the cement* on strength development can also partly be carried back to a geometrical problem, since it appears that the effect of the clinker composition on strength can be considered in terms of variations in the rate of hydration and of structural formation rather than in terms of dramatic changes in the physico-chemical structure of the cement paste. This fact reduces the need for chemistry-oriented, empirical formulae for the prediction of strength as proposed by, for example, Popovics [49]. It compels, however, to investigations on the effect of the chemical composition of the cement on the development of the pore structure of the paste and of the gel structure.

Interface Aspects

Differences between the structure of bulk paste, on the one hand, and interface paste, on the other, can be explained partly from a physico-chemical point of view and partly from a stereological standpoint. The stereological part refers to the "wall effect" as it occurs at the aggregate surface immediately after mixing of the cement with water and aggregate. Around the aggregate surface a water-rich zone forms which results in an interface layer with high porosity and a relatively low strength. The thickness of the interfacial zone has been reported to vary from 20 to 50 μm and even more, depending on the fineness of the cement and, above all, on the w/c ratio. For a survey of interfacial aspects, see [4].

2.8   *Degree of Hydration*

To what extent the hydration process has proceeded is usually indicated with the term "degree of hydration". For several reasons an unambiguous definition of the degree of hydration is hard to give, if not impossible. The ultimate stage of complete hydration has trivially been defined as the stage in which all the cement has reacted. Although trivial, it is still not easy to determine when in a poly-size and poly-mineral specimen all the material has reacted. In this respect one should remember that the chemical composition of cement particles varies with the particle size and that different constituents do not hydrate at the same rate. Moreover, different constituents neither produce equal amounts of heat of hydration nor do they bind equal amounts of water per unit weight. *In spite of all these difficulties we are nevertheless inclined to define the degree of hydration* $\alpha(t)$ *as the ratio between the amount of cement that has reacted, i.e. that has been dissolved, at time t relative to the original amount of cement.* In other words (see also [50]):

$$\alpha(t) = \frac{amount\ of\ cement\ that\ has\ reaction\ at\ time\ t}{total\ amount\ of\ cement\ at\ time\ t = 0} \tag{2.1}$$

The charm of this definition is, as will be shown in subsequent chapters, its relative convenience in the case of considerations concerning the stereological aspects of structural formation.

In the following the degree of hydration is assumed to be identical with the degree of heat liberation. For a more detailed survey of parameters with which the degree of hydration can be approximated and accuracy considerations reference is made to [4].

14

2.9 Kinetics and Rate Formulae

At the end of the summary of factors and aspects involved in hydration and microstructural development and as an introduction to the next chapter some remarks are made as regards kinetics. In this respect it is worthwhile to recall in mind that the reaction of cement with water is very complex. It is a heterogeneous reaction of the general form [16, 51]:

$$\text{solid A} + \text{liquid B} = \text{solid C} \tag{2.2}$$

The complexity of heterogeneous reactions and the relative exactness of mathematical models and rate formula has been discussed extensively by Hakvoort [53]. Unlike homogeneous reactions, i.e. liquid and gas reactions heterogeneous reactions are much more complex because of particle size effects. In the case of cement hydration, the poly-mineral character of the reactant is another complicating factor with respect to the accuracy of mathematical modelling of reaction kinetics. For all these reasons one has to realize that the observed kinetics of heterogeneous reactions in poly-size and poly-mineral systems mirror an *average* or *combined* result of different reactions, processes and phenomena involved in the hydration process.

Kinetic models for cement hydration can be subdivided in roughly four classes. At first one can distinguish between models which describe *overall kinetics* and models which particularly focus on *particle kinetics*. A third class is formed by *hybrid kinetic models*. In this study emphasis will be on what has been termed *integrated kinetic models*.

Overall Kinetics

Among the chemistry-oriented models and rate formulae the Avrami-Erofeev and Kolmogoroff-Erofeev formulae must be mentioned. In these formulae the effect of the particle size distribution and of the development of interparticle contacts on the rate of hydration is allowed for implicitly in the experimentally obtained formula constants.

Particle Kinetics

The importance of the particle size distribution of the cement on the rate of hydration has been emphasized in classical papers of Kondo et al. [54], Taplin [55] and, later, Bezjak [56] and Knudsen [57]. As regards the type of reaction the first authors distinguished between, among other things, boundary and diffusion controlled reactions. In the diffusion layer, formed by the reaction products, there has been distinguished between *inner* and *outer* product, for which different diffusion coefficients would hold. Pommersheim [58] furthermore considered an *intermediate* layer, which would gradually disappear with increasing degree of hydration. A decrease of the diffusion coefficient with increasing degree of hydration, as observed in many tests, has been ascribed to densification of the gel due to merging of hydration products when formed in an increasingly confined space [59].

Hybride Kinetics

The term hybrid kinetics is used for models in which particular features of particle

kinetics, and hence of the particle size distribution, as well as effects of both the state of water in the pore system and the chemical composition of the cement are dealt with in one way or another. Models of this type are those presented by Parrott [60], Knudsen [57, 61], Bezjak et al. [56, 62, 63], Pommersheim [64, 65] and Röhling [66].

Integrated Kinetics
In afore mentioned models microstructural development and the effect of it on the rate of hydration are not considered explicitly. Explicit modelling of interferences between processes, mechanisms and reactions involved in the hardening of a poly-size and poly-mineral cement-water system is, in essence, a prerequisite for consistent modelling and is certainly one of the major challenges for the computational materials science. Maybe Frohnsdorff [67] was among the first who outlined the structure of a numerical model with which hydration and microstructural development of a cement paste could be simulated more or less comprehensively. The vast potentialities of modern computers to simulate the complex and mutually interrelated processes and mechanisms occurring in hardening cement based materials have been emphasized more recently by Jennings [6]. Recent work of Garbozci [68] and Bentz et al. [69] is to be considered as a detailed elaboration of the computer-based approach on a fundamental and most promising basis.

3   HYMOSTRUC: Numerical Model for Hydration and Micro-Structural Development

3.1   *Philosophy Behind the Simulation Model*

In the computer-based simulation model HYMOSTRUC the effects of particle size distribution, the w/c ratio, the reaction temperature and the interaction between hydrating cement particles on the rate of hydration of individual cement particles, are modelled explicitly. For that purpose the development of microstructure is considered to be a process of formation of contacts between expanding cement particles. With progress of the hydration process small particles, located in the close vicinity of bigger particles, will gradually become engulfed by, and embedded in, the outer shell of the latter. The formation of interparticle contacts as indicated here is considered the basis for numerical simulation of microstructural development.

Since explicit modelling of microstructural development and of the interaction between the rate of reaction and microstructural development is one of our major aims, due attention is to be given to the stereological aspect of the hardening process. In this respect the particle size distribution and the spatial distribution of particles in the paste has to be dealt with.

3.2   *Stereological Aspects*

3.2.1   Paste Characteristics

At the present stage of development HYMOSTRUC concentrates on the simulation of

16

hydration and structural development of *bulk cement pastes*. Some of the paste characteristics often used in this papers are described in the following.

Specific Mass

For the specific mass ϱ_{pa} of a cement paste with w/c $= \omega_0$ it holds (no air volume considered):

$$\varrho_{pa} = \frac{\varrho_{ce} * (1 + \omega_0)}{1 + \varrho_{ce} * \omega_0} \quad [g/cm^3] \tag{3.1}$$

(Volumetric) Paste Density

The paste density ζ_{pa} is defined as the cement volume relative to that of the fresh paste:

$$\zeta_{pa} = \frac{G(\infty)}{\varrho_{ce} * V_{pa}}$$

where:

$$V_{pa} = G(\infty) * [1/\varrho_{ce} + \omega_0/\varrho_w] \quad [cm^3] \tag{3.2}$$

With $G(\infty) = 1$ g and $\varrho_w = 1$ g/cm^3 it follows:

$$\zeta_{pa} = [1 + \varrho_{ce} * \omega_0]^{-1} \quad [\mu m^3/\mu m^3] \tag{3.3}$$

Fig. 3.1 shows the volumetric paste density as a function of the w/c ratio.
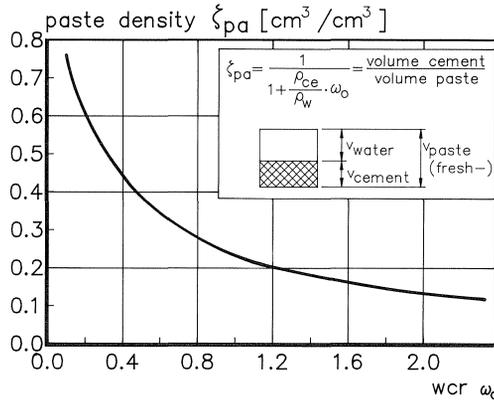
Fig. 3.1 Volumetric paste density ζ_{pa} as a function of the w/c ratio.
Note: The curve in this figure refers to fresh paste!

3.2.2 Particle Size Distribution

For the particle size distribution of the cement the Rosin-Rammler distribution is adopted. In formula form:

$$G(x) = 1 - e^{-bx^n} \quad [g] \tag{3.4}$$

17

in which x [μm] is the particle diameter and b and n constants which are determined so that $G(x \to \infty) = 1$ g. The cement particles are assumed to have a spherical shape. It must be noticed that the adopted particle shape has a bearing on the interpretation of hydration data. For a detailed discussion on interpretation problems caused by the particle shape reference is made to [4].

3.2.3 Cell Definition. Cell Volume and Particle Spacing

The mean spacing L_x between particles belonging to fraction F_x in a mix with w/c ratio ω_0 can be estimated by assuming that the particles under discussion are situated in the centre of a cube-shaped "cell". For a cell the following definition holds:

"Cell definition"
A cell "I_x^c" is defined as a cubic space in which the largest cement particle has a diameter x, and further consists of $1/N_x$ times the original water volume and of $1/N_x$ times the volume of all particles with diameter smaller than that of particle x (Fig. 3.2):

$$I_x^c = (V_w + V_{\leq x}) * N_x^{-1} \quad [\text{cm}^3] \tag{3.5}$$

where:

$$V_w \quad = \text{initial water volume} = [\omega_0 * G(\infty)]/\varrho_w \quad [\text{cm}^3]$$
$$V_{\leq x} \quad = G(x)/\varrho_{ce} = \text{cement volume of particles} \leq x \quad [\text{cm}^3]$$
$$\varrho_w, \varrho_{ce} = \text{specific mass in g/cm}^3 \text{ of water and cement}$$
$$N_x \quad = \text{number of particles with diameter } x \text{ μm}$$
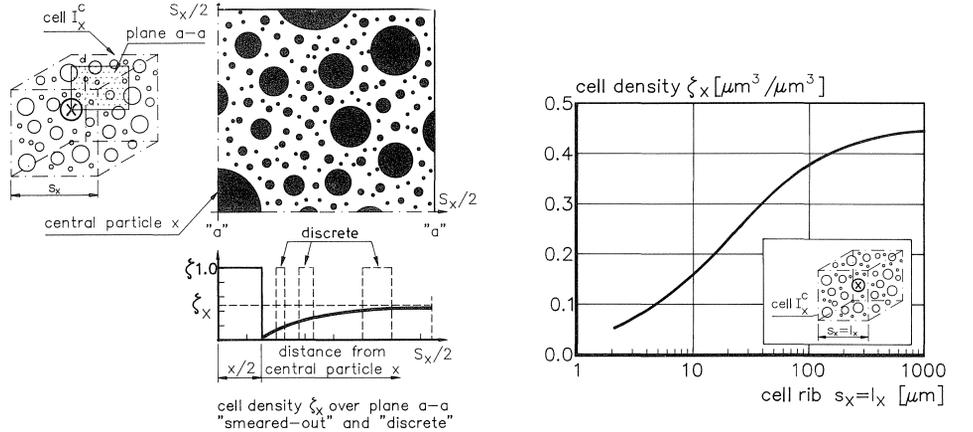
Fig. 3.2   a. Schematic representation of the cell density as a function of the distance from the outer surface of a spherical central particle.
        b. Cell density as a function of rib size of the cell; Blaine ≈ 350 m²/kg.

The mean centre-to-centre particle spacing L_x [μm] is assumed to be equal to the rib size S_x of the cubic cell I_x^c (for detailed considerations, see [70]):

$$L_x = S_x = [I_x^c * 10^{12}]^{1/3} \quad [\text{μm}] \tag{3.6}$$

18

Since the cell volume I_x^c is a function of both the w/c ratio and the particle size distribution, the particle spacing L_x is a function of these parameters as well. For an indication of the particle spacing, reference is made to Fig. 3.3. The figure clearly demonstrates that even in the case of low w/c ratios the average particle spacing L_x of particles belonging to fraction F_x substantially exceeds the particle diameter x.
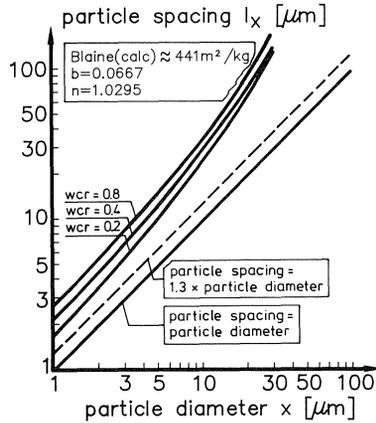
Fig. 3.3 Particle spacing as a function of the w/c ratio. Blaine ≈ 440 m²/kg.

3.2.4 Shell Density

On the basis of the assumed homogeneous spatial distribution of the cement particles in the paste it is relatively easy to determine the amount of cement found in a fictitious shell with shell thickness d surrounding an arbitrary cement particle with diameter x μm. For this purpose a *shell density factor* $\zeta_{sh;x,d}$ of an outer shell with thickness d has been defined, viz.:

$$\zeta_{sh;x,d} = \frac{\text{cement volume in spherical shell with thickness } d}{\text{total shell volume}} \tag{3.7}$$

A diagrammatical representation of the shell density factor is shown in the bottom part of Fig. 3.2a. Going from the periphery of particle x in outward direction the shell density gradually increases from zero just at the outer periphery of the anhydrous particle to the paste density ζ_{pa} according to equation (3.3). For details about the numerical evaluation of the shell density factor reference is made to [4].

The introduction of the shell density concept allows to calculate the amount of cement met by the outer products of a hydrating and expanding central particle and, moreover, to calculate the effect of particle interaction on the rate of hydration.

3.3 *Interaction Mechanisms*

3.3.1 Introductory Remarks

In the foregoing cement particles of the same size were assumed to be located at equal

19

distances from each other. This approach has significantly simplified the determination of the amount of cement found in a fictitious shell around an arbitrary cement particle x. In reality, however, the particles are located randomly in the system and a probabilistic approach would, therefore, be more suitable to characterize the stereological distribution of the particles in the system. This would also be a more realistic starting point for simulating the development of a microstructure during the hydration process. In [4] it has been explained that, if we would allow for the actual randomness of the particle distribution of the cement, numerical simulation of even a small poly-size cement sample would result in huge computation times. In case of a random distribution each particle would then have a unique position in the paste. This unique position implies that also the rate of hydration of each particle will be affected by its neighbour particles in a unique way. This, on its turn, will result in a unique rate of hydration of each individual particle. Hence, the progress of the hydration process of each individual particle would have to be followed, resulting in aforementioned huge computation times. Adoption of a homogeneous distribution of the particle in the paste, on the contrary, implies that particles of the same size interfere with neighbour particles in the same way and hydrate, consequently, at the same rate.

Anticipating on the derivations in subsequent sections it is emphasized here, that in considerations concerning the degree of hydration of the amount of cement present in a fictitious shell around particle, this cement is considered to consist of particles with diameters in the range from 1 to $(x - 1)$ μm. In this way it is still possible to simulate that *also* particles of approximately the same size directly interfere with each other during the hydration process. In this more probabilistic-oriented part of the calculations the position of the particles in the paste is *not* defined explicitly. A consequence of this is, that the number of particles involved in the interaction process must be counted carefully on penalty of counting them more than once.

3.3.2 Basic Assumptions

Against the background of and in addition to the introductory remarks in Section 3.3.1, four basic assumptions are made in order to achieve to a workable algorithm for determination of the physical interaction between hydrating cement particles.

1. Particles belonging to the same fraction hydrate at the same rate.
   Comment: It is obvious that a small particle which is completely surrounded in the liquid phase will hydrate in a different way, and probably at a different rate, than a particle of the same size but located close to the surface of a large particle. As explained in the foregoing section, however, accounting for different rates of hydration of individual particles of the same fraction would increase the calculation effort tremendously.

2. For isothermal curing the ratio v between the volume of the gel and that of the reactant is assumed to be a constant throughout the hydration process.

20

Comment: A constant value of the parameter v in mathematical modelling has also been used, in the absence of reliable experimental data, by Pommersheim [59]. For indicative values of v reference is made to [4].

As suggested with the formulation of this second basic assumption *non-isothermal* effects will be considered differently, i.e. with a temperature dependent value of the ratio under consideration. A proposal for a temperature-dependent value of v, i.e. $v = v(T)$, reference is made in Section 3.4.2.4.

3. Reaction products precipitate in the close vicinity of the cement particles from which they are formed.
   Comment: The reaction products are assumed to build up a gel of constant density. This assumption is based on the "unstable pore concept" suggested by Powers [24] and also adopted by Granju et al. [38].

4. The development of internal stresses associated with formation of microstructure is not considered explicitly.
   Comment: Chemical shrinkage is considered to cause internal stresses and microcracking [7]. Both hydration under pressure and the process of microcracking might affect the rate of hydration. The effect of these processes are implicitly allowed for, in part, in the value of the *"independent model parameters"* to be discussed in detail in Section 3.4.3.

With these basic assumptions the framework has been established within which the simulation model will be developed. To avoid confusion it will be emphasized here that these basic assumptions refer to a *model,* and should not be interpreted as conclusions with regard to the far more complex reality of hydrating poly-mineral and poly-size two-phase systems!

3.3.3   Mechanism of Particle Expansion during Hydration

To explain the interaction mechanism that occurs around a hydrating particle x, the progress of the hydration process and associated expansion of this particle will be followed. An arbitrary stage in the hydration process is shown diagrammatically in Fig. 3.4. In this stage, i.e. at time $t = t_j$, the degree of hydration of particle x is $\alpha_{x,j}$. For the corresponding *penetration depth* $\delta_{in;x,j}$ of the reaction front it holds that:

$$\delta_{in;x,j} = \left(\frac{x}{2}\right) * \left[1 - \{1 - \alpha_{x,j}\}^{1/3}\right] \tag{3.8}$$

The volume of the outer product $v_{ou;x,j}$ that corresponds to the degree of hydration $\alpha_{x,j}$ is:

$$v_{ou;x,j} = (v - 1) * \alpha_{x,j} * v_x \tag{3.9}$$

Absence of cement in the shell surrounding particle x would lead to free expansion of this particle. As a result, the outer radius $R_{ou;x,j}$ of the expanding central particle would be:

$$R_{ou;x,j} = \left[\frac{v_{ou;x,j}}{\frac{4\pi}{3}} + \left(\frac{x}{2} \right)^3 \right]^{1/3} \tag{3.10}$$

For the thickness $\delta_{ou;x,j}$ of the outer shell it follows (see Fig. 3.4a):
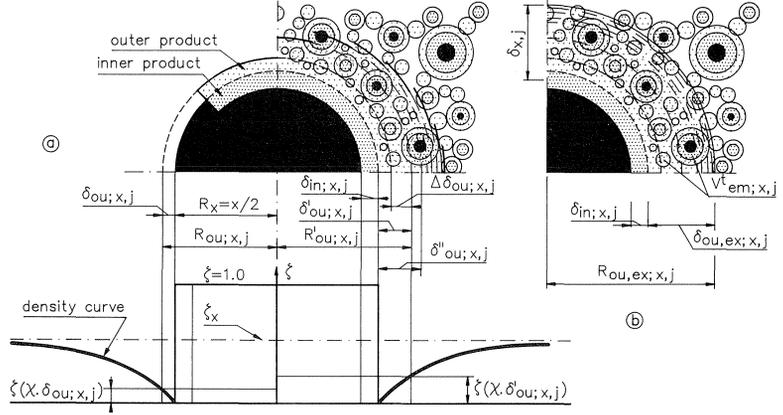
Fig. 3.4   Interaction mechanism for expanding particles.
a. Left part: free expansion. Right part: particle embedding, several iteration steps.
b. Expansion affected by embedding of small particles; final stage (one time step).

$$\delta_{ou;x,j} = R_{ou;x,j} - \frac{x}{2} \tag{3.11}$$

In reality the outer shell is partly filled with embedded cement particles. The volume of the cement in the outer shell with thickness $\delta_{ou;x,j}$, which volume is called the *directly embedded cement volume* $v_{em;x,j}$, can be determined by multiplying the shell volume $v_{ou;x,j}$ with the shell density factor $\zeta_{sh;x,d} = \zeta(\chi \cdot \delta_{ou;x,j})$ according to equation (3.7):

$$v_{em;x,j} = \zeta(\chi \cdot \delta_{ou;x,j}) * v_{ou;x,j} \tag{3.12}$$

in which $d = \delta_{ou;x,j}$ is the thickness of the outer shell at time t_j and χ a *stereometric conversion factor,* allowing for a change from a cubic to a spherical shape of a cell. For this conversion factor is hold $\chi = [4\pi/3]^{1/3}$ [4].
The directly embedded cement volume is built up of particles smaller than x μm and is partly hydrated. In the partly hydrated state the volume of the directly embedded cement at time $t = t_j$ can be calculated using (see Fig. 3.4b):

$$v_{em;x,j,\alpha} = v_{em;x,j} * (1 - \alpha_{<x,j}) + v_{em,x,j} * \alpha_{<x,j} * v$$

or:

$$v_{em;x,j,\alpha} = v_{em;x,j} * \{(1 + (v - 1) * \alpha_{<x,j}\}$$

The embedded and partly hydrated cement volume accounts for an *additional* expan-

22

sion of the outer shell of particle x. For the total volume of the additionally expanded outer shell it follows:

$$v'_{ou;x,j.} = v_{ou;x,j} + v_{em;x,j,a}$$

The outer radius $R'_{ou;x,j}$ of the extra expanded outer shell is now:

$$R'_{ou;x,j} = \left[\frac{v'_{ou;x,j}}{\frac{4\pi}{3}} + \left(\frac{x}{2}\right)^3 \right]^{1/3}$$

For the new thickness of the outer shell it follows:

$$\delta'_{ou;x,j} = R'_{ou;x,j} - \frac{x}{2}$$

With the extra increase of the shell thickness, viz.:

$$\Delta\delta_{ou;x,j} = \delta'_{ou;x,j} - \delta_{ou;x,j}$$

the amount of embedded cement will increase as well. The amount of cement found in the shell with a thickness $\Delta\delta_{ou;x,j}$ is called *indirectly embedded cement volume*. The total of directly and indirectly embedded cement volumes can be calculated in a way analogous to the calculation of the directly embedded cement volume. From comparison with equation (3.12) it follows:

$$v'_{em;x,j} = \zeta(\chi \cdot \delta'_{ou;x,j}) * v'_{ou;x,j}$$

Since $\delta'_{ou;x,j} > \delta_{ou;x,j}$, the value of $\zeta(\chi \cdot \delta'_{ou;x,j})$ will be slightly higher than the value of $\zeta(\chi \cdot \delta_{ou;x,j})$ (bottom part of Fig. 3.4a). Consequently, the total volume of embedded cement will increase. The extra embedded cement in turn causes another extra increase of the outer shell, etc. This expansion mechanism, which is inherent in the spatial composition of the hydrating system, on the one hand, and to the adopted constancy of the volume ratio v between reaction products and reactant, on the other, finally results in the following geometrical series:

$$v^n_{ou;x,j} = v_{ou;x,j} + \left[1 + \zeta(\chi \cdot \delta^n_{ou;x,j}) * \{1 + (v-1) * \alpha_{<x,j}\}^1 + \right.$$
$$+ \zeta(\chi \cdot \delta^n_{ou;x,j}) * \zeta(\chi \cdot \delta^{n-1}_{ou;x,j}) * \{1 + (v-1) * \alpha_{<x,j}\}^2 +$$
$$\left. + \zeta(\chi \cdot \delta^n_{ou;x,j}) * \zeta(\chi \cdot \delta^{n-1}_{ou;x,j}) * \zeta(\chi \cdot \delta^{n-2}_{ou;x,j}) * \{1 + (v-1) * \alpha_{<x,j}\}^3 + ... \right]$$

Unfortunately the geometrical ratio of this series is not a constant. In most cases, however, and certainly at the start of the hydration process, the directly embedded cement volume is much larger than the indirectly embedded cement volume. It can, therefore, be assumed that for the calculation of the indirectly embedded cement volume the shell density $\zeta(\chi \cdot \delta_{ou;x,j})$, which belongs to the initial outer volume $v_{ou;x,j}$ of particle x, can be adopted. Under this condition the geometrical ratio r of the series becomes:

$$r = \zeta(\chi \cdot \delta_{ou;x,j}) * \{1 + (v-1) * \alpha_{<x,j}\}$$

For the *volume of the expanded outer shell,* $v_{ou,ex;x,j}$, it then follows:

$$v_{ou,ex;x,j} = \frac{v_{ou;x,j}}{1 - \zeta(\chi \cdot \delta_{ou;x,j}) * \{1 + (\nu - 1) * \alpha_{<x,j}\}} \tag{3.13}$$

For the outer radius of the expanded outer shell we obtain (Fig. 3.4b):

$$R_{ou,ex;x,j} = \left[\frac{v_{ou,ex;x,j}}{\frac{4\pi}{3}} + \left(\frac{x}{2}\right)^3 \right]^{1/3} \tag{3.14}$$

while for the thickness of the expanded outer shell it holds that:

$$\delta_{ou,ex;x,j} = R_{ou,ex;x,j} - \frac{x}{2} \tag{3.15}$$

With equation (3.8) and equation (3.15) the total thickness $\delta_{x,j}$ of the shell which surrounds the shrinking anhydrous core is:

$$\delta_{x,j} = \delta_{in;x,j} + \delta_{ou,ex;x,j} \tag{3.16}$$

For the total embedded cement volume $v_{em;x,j}^t$, i.e. the sum of directly and indirectly embedded, partly hydrated, cement volume it follows:

$$v_{em;x,j}^t = v_{ou,ex;x,j} - v_{ou;x,j} \tag{3.17}$$

This embedded cement, consisting of particles with a diameter smaller than x, is hydrated up to a degree $\alpha_{\leq x,j}$. For the original volume of embedded cement, i.e. the cement volume in its anhydrous state, $v_{em;x,j}^0$, it holds that:

$$v_{em;x,j}^0 = \frac{v_{em;x,j}^t}{1 + (\nu - 1) * \alpha_{\leq x,j}} \tag{3.18}$$

Indicative values

Indicative values for the volume of the embedded cement will be given in Section 4.2.2. For orientation: for a particle with diameter $x = 16$ µm and a volume of 2,144 µm^3, hydrating in a system with a w/c ratio of 0.4 the maximum amount of directly and indirectly embedded, partly hydrated cement has been calculated at about 1,000 µm^3.

3.3.4 Embedded and Free Particles

3.3.4.1 Number of Embedded and Free Particles

With increasing degree of hydration more particles become embedded in the expanding outer shells of large particles. Hence, the number of hydrating "free clusters" decreases with time. The number of free particles $N_{x;fr}$, i.e. free clusters with a central particle x, consists of the original number of particles N_x of fraction F_x *minus* the particles of this fraction embedded in the outer shells of particles larger than x µm.

3.3.4.2 Embedded Centre-Plane Area and Contact Area

The cement volume embedded in the outer shell of particle x consists, by definition, of particles with diameter smaller than x μm. As mentioned earlier already small particles, say particles with diameter $x \leq x_{dis} \approx 3$ μm, completely dissolve and hence lose their geometrical identity. These particles only contribute to an extra outward growth of the outer shell of the central particle. Larger particles, with diameters up to x μm, can be either fully or partly embedded in the outer shell or particle x. For particles with a diameter exceeding the thickness of the outer shell $\delta_{ou,ex;x}$, it is only possible that these are partly embedded. It is assumed that the larger embedded particles, and in particular the particles with a diameter exceeding the outer shell thickness, are able to bridge the interparticle distances between adjacent expanding particles and hence determine the strength of the cement paste. This concept is diagrammatically shown in Fig. 3.5. Within the boundaries of this concept it can be expected that the total centre-plane area of particles which bridge the interparticle distances will show a more or less distinct correlation with strength.
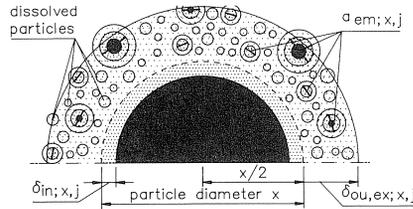
Fig. 3.5   Definition and formation of contact area; conceptional (For $a_{em;x,j}$, see text).

For complete mathematical procedures for the determination of the embedded centre-plane area reference is made to [4]. For the total embedded centre-plane area $A_{em;j}$ of the hydrating system as a whole, i.e. a paste made with 1 g cement, at time t_j it holds (disregarding the contribution of particles smaller than x_{dis}):

$$A_{em;>x_{dis},j} = \sum_{x=(x_{dis}+1)}^{x_{max}} a_{em;x,j} \cdot N_{x;fr,j} \quad [\mu m^2/g \text{ cement}] \tag{3.19}$$

where $a_{em;x,j}$ is the embedded centre-plane area of particles smaller than x μm embedded in the outer shell of particle x at time t_j and $N_{x;fr,j}$ the number of free particles, or free clusters, in fraction F_x with central particles x at time t_j.

3.4 *Rate of Penetration of the Reaction Front*

3.4.1 General

In the foregoing Sections the stereological aspect of hydration has been dealt with. It was shown how expanding particles will embed smaller particles, the latter either fully or partly hydrated. In this Section the rate of hydration will be discussed. The elaborated so called *Basic Rate Equation* the rate of penetration of a reaction front is

25

determined and covers the initial *Phase-Boundary Reaction* and the *Diffusion Controlled Reaction*. Particular attention will be given to the effect of particle interaction on the rate of hydration.

3.4.2 Basic Rate Equation

For the determination of an incremental increase of the penetration depth $\Delta\delta_{in;x,j+1}$ of particle x during a time increment $\Delta t_{j+1} = t_{j+1} - t_j$ a penetration formula is proposed, which in its basic form is as follows:

$$\Delta\delta_{in;x,j+1} = \{\Delta\delta_{in;x,j+1}\}_0 * \Omega_1(x, \alpha_{x,j}) \quad [\mu m/hr] \tag{3.20a}$$

with:

$$\{\Delta\delta_{in;x,j+1}\}_0 = \frac{K_i(\alpha_j) * F_1(\cdot) * (F_2(\cdot))^\lambda * \Omega_2(\cdot) * \Omega_3(\cdot)}{\{(\delta_{x,j})^\lambda\}^{\beta_1}} \cdot \Delta t_{j+1} \tag{3.20b}$$

where:

K_i = rate constant, depending on the rate-controlling mechanism, cement composition and degree of hydration
$i = 0$ in case of phase-boundary reaction $[\mu m/h]$
$i = 1$ in case of diffusion-controlled reaction $[\mu m^2/h]$

$F_1(\cdot) = F_1(T, \alpha, C_3S)$ = "net" temperature function, accounting for the effect of the curing temperature on the rate of processes

$F_2(\cdot) = F_2(T, \alpha, C_3S)$ = temperature function, accounting for effect of curing temperature on morphology and formation of structure. Operative only in diffusion stage

$\Omega_1(x, \alpha_{x,j})$ = reduction or *partition factor,* accounting for water withdrawal effects as occurring for a particle with diameter x (see Section 3.4.2.2)

$\Omega_2(\alpha_j)$ = reduction factor, accounting for water shortage in the pore system (overall effect)

$\Omega_3(\alpha_j)$ = reduction factor, accounting for reduction of the *amount* of water in the hydrating mass (overall effect)

λ = factor, depending on the rate-controlling mechanism
$\lambda = 0$ for phase-boundary reaction
$\lambda = 1$ for diffusion-controlled reaction

β_1 = a constant, to be determined from suitable tests

$\delta_{x,j}$ = total thickness of product layer $[\mu m]$ of particle with diameter x at the end of time step Δt_j

Particular features of the rate constants K_i, reduction factors $\Omega_1(\cdot)$, $\Omega_2(\cdot)$ and $\Omega_3(\cdot)$ and temperature functions $F_1(\cdot)$ and $F_2(\cdot)$ are discussed in subsequent sub-sections.

3.4.2.1 Basic Rate Factors K_i and Transition Thickness δ_{tr}

The change from a phase-boundary to a diffusion-controlled reaction would occur at an overall degree of hydration $\alpha \approx 0.2$ (see [4]). Depending on the fineness of the cement the corresponding penetration depth is then about 2...3 μm. For this value of the penetration depth the degree of hydration of individual particles will differ quite significantly. Small particles will be fully hydrated already, whereas large particles are hydrated by only a few percent. It would not be correct, therefore, to relate the change from phase-boundary reactions to diffusion-controlled reactions to a fixed value of the degree of hydration. Instead of a transition value of the *degree of hydration* it is proposed to correlate the moment of the change of the rate-controlling mechanism to the thickness of the diffusion layer, i.e. to a *"transition thickness δ_{tr}"*. It is further assumed that this change takes place gradually. This assumption can be allowed for by equalizing the rates of hydration, i.e. the rates of penetration, for both the phase-boundary reaction and the diffusion reaction at the moment when the thickness of the product shell has reached the transition thickness (Fig. 3.6). The required equal rates of penetration directly prior and after the transition point determine a relationship between the rate constants K_0 and K_1 of equation (3.20b). Thus:
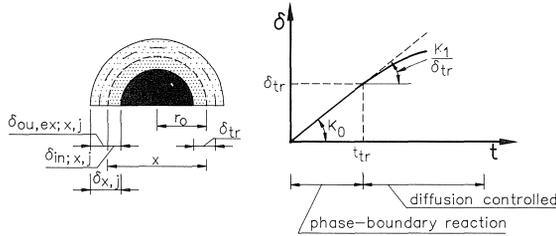
Fig. 3.6   Change of rate-controlling processes; schematic presentation.

$$\frac{\{\Delta \delta_{in;x,j+1}\}_0}{\Delta t_{j+1}} = \frac{K_0 * F_1(\cdot) * (F_1(\cdot))^{\lambda=0} * \Omega_2(\cdot) * \Omega_3(\cdot)}{\{(\delta_{x,j})^{\lambda=0}\}^{\beta_1}} =$$

$$\frac{K_1 * F_1(\cdot) * (F_2(\cdot))^{\lambda=1} * \Omega_2(\cdot) * (\Omega_3(\cdot)}{\{(\delta_{x,j})^{\lambda=1}\}^{\beta_1}}$$

At the transition point, when $\delta_{x,j} = \delta_{tr}$, then (for $F_1(\cdot) = 1$):

$$K_1 = K_0 * \{\delta_{tr}\}^{\beta_1} \tag{3.21}$$

Transition Thickness. Tentative Values
An indication of the magnitude of the transition thickness δ_{tr}, and hence of the ratio K_1/K_0, can be deduced from data presented by Bezjak et al. [56, 63] and Alujevic et al. [72].
According to Alujevic, investigating a hydrating CaO-quartz system, the ratio K_1/K_0 ranges from 1.76 to 3.26. Similar investigations, carried out by Bezjak et al. with Portland cement pastes, revealed a K_1/K_0 ratio between 2.35 and 3.43. From equation (3.21)

27

it follows that for $\beta_1 = 1$ these K_1/K_0 ratios can be interpreted as transition thicknesses δ_{tr} [µm]. These values are in good agreement with the value $\delta_{tr} = 2.6$ µm derived from Bezjak's data.

These considerations undeniably show distinct trends regarding the transition thickness of the diffusion layer. When quantifying the transition thickness δ_{tr} (Section 3.4.3) values in the range from 1.5 to 4 µm can be expected.

It is noticed here already that good predictions with the simulation model are obtained with values for $\beta_1 = 1...2$. Values of $\beta_1 > 1$ suggest a higher K_1/K_0 ratio, the value of δ_{tr} being the same. Higher values of β_1, however, reveal to be associated with lower values of the transition thickness δ_{tr}. Hence, the ratio between K_1 and K_0 still remains varying in the range just indicated.

It should be noted that the results obtained by Alujevic and Bezjak have shown, that with an increase of the degree of hydration the ratio K_1/K_0 increases as well. A possible interpretation of this result is, that during the hydration process diffusion through the outer shell becomes increasingly difficult, i.e. merging of outer products of mutually interfering particles becomes of paramount importance.

Furthermore it should be noted that the degree of hydration, i.e. the depth of penetration, at which the change of rate-controlling mechanisms takes place roughly coincides with the stage in the hydration process in which the ion concentration in the liquid phase significantly changes [4]. This makes it hard to deduce from experimental data which phenomenon is responsible for changes in the rate of hydration associated with the change from a phase-boundary reaction to a diffusion controlled reaction.

Overall Degree of Hydration
It is considered evident that the overall degree of hydration α_j at time t_j can be obtained by summarising the contribution to this quantity of the individual cement particles, i.e. individual fractions. For numerical evaluations in this respects reference is made to [4].

3.4.2.2   Effects of Particle Interaction on the Rate of Penetration

The consequence of the embedding of particles in the outer shell of a hydrating central particle on the rate of penetration is *two-fold*. Firstly, extra expansion of the outer shell will cause a decrease of the diffusion rate. Secondly, water withdrawal will occur due to the presence of incompletely hydrated particles in the outer shell of the central particle considered.

Increased Shell Expansion
Initially the extra thickening of the outer shell occurs as discussed in Section 3.4.2.1. An extra expansion implies a higher diffusion resistance for ions or particles moving to and from the anhydrous core of the central particle and an associated decrease of the rate of penetration. The effect of extra shell expansion due to particle embedding will be elucidated in detail in Sections 4.2.2 and 4.3.

28

Water Withdrawal by Embedded Particles: Reduction Factor $\Omega_1(x, a_{x,j})$

The second factor refers to the hydration of embedded and still incompletely hydrated particles. A consequence of the first basic assumption made in Section 3.3.2, viz. the assumption of an equal degree of hydration of particles which belong to the same fraction, is that the embedded and still hydrating particles will withdraw a certain amount of the water $\Delta w_{em;x,j}$ needed for further hydration of the central particle. For the hydrating central particle an amount of water $\Delta w_{x,j+1}$ is available for the reaction in the subsequent time step Δt_{j+1}. The water withdrawal mechanism is diagrammatically shown in Fig. 3.7. The resulting decrease of the rate of penetration of the reaction front in particle x is accounted for with the reduction factor $\Omega_1(.) = \Omega_{em;x,\alpha}$.

a. No water withdrawal   b. Water withdrawal considered
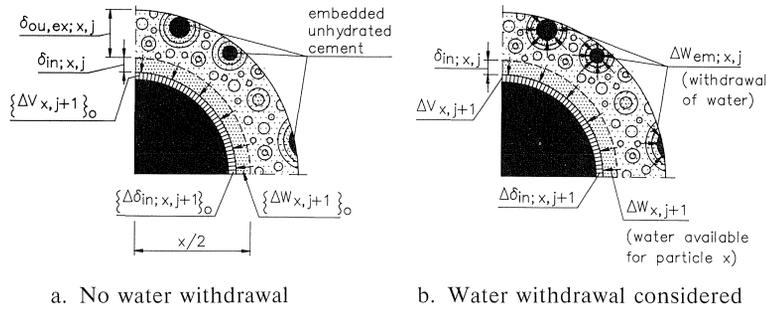
Fig. 3.7   Effect of embedded particles on the rate of hydration. Water withdrawal, schematic.

For three particle sizes, viz. $x = 20, 40$ and $110\ \mu m$, the reduction factors $\Omega_1(\cdot)$ are given in Fig. 3.8 for a paste with $\omega_0 = 0.4$. For low w/c ratios the reduction factors for large particles may approach zero because most of the water needed for further hydration of the latter is used up by the embedded small particles.
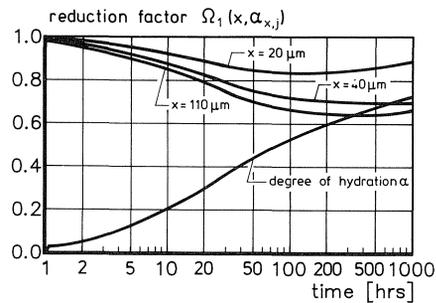
Fig. 3.8   Reduction factor $\Omega_1(x, \alpha_{x,j})$ accounting for water withdrawal by embedded particles [4] ($\alpha = $ overall degree of hydration).

3.4.2.3   Water Shortage Effects. State of Water in Pore System

Effect of Water Shortage in the Pore System. Reduction Factor $\Omega_2(\alpha_j)$

During the hydration process the capillary pores are gradually emptied until a thermo-

dynamic equilibrium is reached. This state of equilibrium depends on the relative humidity in the pore system, the pore size distribution and the pore size. In any intermediate stage of equilibrium the pore system will be filled partly with water and partly with water vapour. Depending on the vapour pressure, i.e. the relative humidity, the walls of the empty pores will be covered with a thin layer of water. According to Hagymassy et al. [73] the average thickness of the adsorption layer decreases steeply from a six mono-molecular layer at RH = 100% to a three mono-molecular layer at RH = 80%. A further decrease of the relative humidity results in a gradual decrease of the layer thickness until a thickness of about 1 mono-molecular layer is reached at RH = 20% (see Fig. 3.9). Assuming that in many practical cases the relative humidity in the pore system does not drop below values of 85 to 90% (see [4]), it can be concluded that at the pore wall an adsorption layer of some thickness will remain. The water in this adsorption layer is assumed to be less easy to mobilize for further hydration.

In view of these considerations the capillary water will be subdivided into *free capillary water* V_{fr} and *adsorbed water* V_{ad} (see also Fig. 3.10):

$$V_{cap} = V_{fr} + V_{ad} \tag{3.22}$$

For the determination of the volume of the adsorption layer with thickness Γ the pore wall area A_{por} of all pores in the range from ϕ_0 to ϕ_{max} has to be determined. The free capillary water will be located in the "remaining pore space", i.e. in the pore space made up of pores which are narrowed by the adsorption layer. The largest pore completely filled with water, ϕ_{wat}, determines the pore wall area A_{wat} that is in contact with free water, i.e. with water that is available for further hydration. It is now assumed that *the fact that a certain amount of the cement matrix is not in direct contact with free water will, in some way, affect the rate of hydration of the system as a whole.* By saying "in some way" one should think in terms of longer distances over which ions involved in the reaction process have to travel from the bulk liquid phase to the anhydrous cement and vise versa.
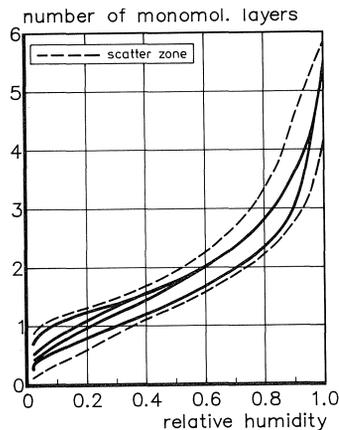
Fig. 3.9   Thickness of adsorption layer as function of the relative humidity [4, 73].
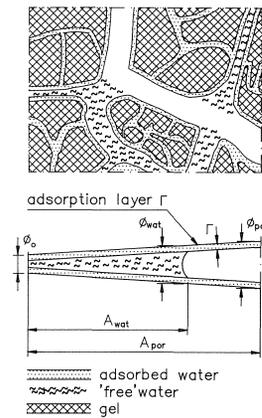
Fig. 3.10   Schematic view of state of water in pore system.

30

To account for the assumed phenomenon a reduction factor $\Omega_2(\alpha_j)$ is proposed as follows (see also Fig. 3.10):

$$\Omega_2(\alpha) = \frac{A_{\text{wat}}(\alpha)}{A_{\text{por}}(\alpha)} \tag{3.23a}$$

in which $A_{\text{por}}(\alpha)$ and $A_{\text{wat}}(\alpha)$ are the total pore wall area and of the wall area of the pores which are completely filled at a degree of hydration $\alpha = \alpha_j$, respectively. Formula (3.23a) can be rewritten as follows:

$$\Omega_2(\alpha) = \frac{\phi_{\text{wat};\alpha} - \phi_0}{\phi_{\text{por};\alpha} - \phi_0} * \frac{\phi_{\text{por};\alpha}}{\phi_{\text{wat};\alpha}} \tag{3.23b}$$

in which $\phi_{\text{wat};\alpha}$ and $\phi_{\text{por};\alpha}$ are the pore diameters of the largest capillary pore which is still completely filled with water and the largest capillary pore in the paste as a whole, respectively. ϕ_0 is the characteristic minimum size of gel pores, i.e. $\phi_0 = 20$ Å.
Indicative values for $\Omega_2(\alpha)$ are shown in Fig. 3.11 for a paste with $\omega_0 = 0.2$ and 0.4. The curves in this figure are obtained for different thicknesses Γ [Å] of the water layer adsorbed at the walls of the empty pores and which thickness is a function of the relative humidity in the pore system. For a three monomolecular water layer with a thickness of about 9 Å the ultimate degree of hydration would not exceed 85%.
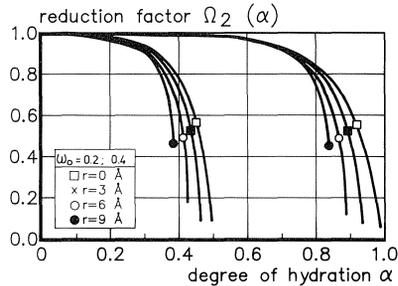
Fig. 3.11   Reduction factor $\Omega_2(\alpha_j)$ as a function of the degree of hydration. Thickness of adsorption layer as parameter [4].

Effect of Reduction of the Amount of Water in the Pore System.
Reduction factor $\Omega_3(\alpha_j)$
Besides the *distribution* of the water also the *amount* of water affects the rate of hydration. This effect is accounted for with the reduction factor $\Omega_3(\cdot) = \Omega_3(\alpha_j)$. The (decreasing) amount of water is a factor in the *dynamic equilibrium* of a process of dissolution of anhydrous cement and precipitation of reaction products. For the effect of the decreasing amount of water on the overall rate of hydration the following expression is postulated, viz. (with $\alpha = \alpha_j$) [4]:

$$\Omega_3(\alpha) = \frac{\omega_0 - 0.4\alpha}{\omega_0} \tag{3.24}$$

31

It is noticed that almost simultaneously with the decrease of the amount of water in the paste a significant change in the ion concentration occurs [74]. Whether this change is the cause or the result of a lower rate of hydration, and how the role of the amount of water has to be valued in this context, is still a point of discussion. More information on interrelated phenomena, processes and mechanisms involved in this stage of hardening is certainly needed.

Comparison of Different Water Shortage Concepts

Literature data on the relationship between the development of the pore size distribution in a hydrating paste and thermodynamically determined relationships between the amount and distribution of pore water in a given pore system on the one hand, and the relative humidity in the empty pores on the other hand, enable us to write the combination factor $\Omega_{23}(\alpha) = \Omega_2(\alpha) * \Omega_3(\alpha)$, written here as a function of the degree of hydration α, in an alternative form, viz. as a function of the relative humidity RH i.e. $\Omega_{23}(RH)$. This enables us to compare the combination factor $\Omega_{23}(RH)$ with similar reduction factors β_{RH} proposed by Parrott [60] and based on work of Bazant/Jonasson [75]. As shown in Fig. 3.12, the Ω_{23}-RH relationship is in good agreement with the reduction factor proposed by Parrott and with experimental data presented by the latter. For the departure of the reduction factor β_{RH} proposed by Bazant/Jonasson from the other proposals no explanation can be given yet.
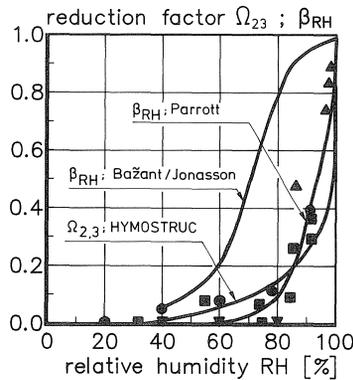
Fig. 3.12 Effect of relative humidity on the rate of hydration. Experimental data indicated with discrete points [4].
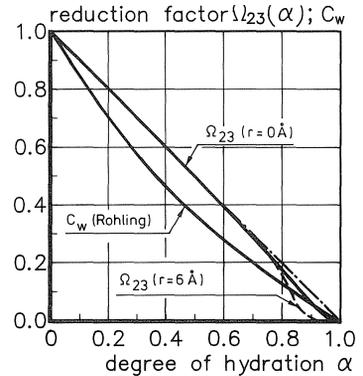
Fig. 3.13 Reduction factor C_w [66] and $\Omega_{23}(\alpha)$ allowing for water shortage in the paste. $\omega_0 = 0.4$.

Röhling [66] has proposed a *water concentration factor* C_w to allow for the effect of water shortage in the pore system. Fig. 3.13 shows the C_w-curve together with two Ω_{23}- curves as a function of the degree of hydration. One Ω_{23}-curve is based on Ω_2-values determined without making allowance for water adsorption at the empty pore walls ($\Gamma = 0$ Å), whereas for the second curve a two monomolecular adsorption layer is considered ($\Gamma = 6$ Å). From a theoretical point of view the second Ω_{23}-α curve should be considered as the most realistic of the two. The curves presented in Fig. 3.13 show that the

32

theoretically determined reduction factor $\Omega_{23}(\alpha)$ is in good accordance with the phenomenological reduction factor C_w found by Röhling.

3.4.2.4 Temperature Dependency of Rate Processes

The rate of most chemical and physical reactions increase with increasing reaction temperature. A well-known rule of thumb says that with an increase of the reaction temperature by 10 °C the rate of reaction increases by a factor 2. This rule has been applied several times and it must be admitted that the results were not always bad [76, 77]. Many experiments, however, have revealed that the rate factor is not a constant, but varies with the *type of cement,* the *reaction temperature* itself and the *degree of hydration.* The major reasons for the complexity of the subject are:
– the poly-mineral character of cement;
– the fact that different reaction mechanisms occur simultaneously;
– the effect of temperature on morphology and structure of the reaction products.
As mentioned in Section 2.3.2 already, the rate of reaction of different constituents differs. Moreover, the morphology of the reaction products differ for different constituents and is also affected by the reaction temperature. The morphology and the thickness of the shell of hydration products which surrounds an anhydrous core in turn determine the moment at which the hydration mechanism changes from a predominantly boundary reaction to a diffusion-controlled reaction. As stated by Bezjak, this moment can in principle be different for different particle sizes [56]. The *temperature sensitivity* of a boundary reaction is known to be higher than that of a diffusion-controlled reaction [20, 51]. Consequently a change of rate determining mechanism will imply a change of temperature sensitivity of the hydrating system. With regard to the diffusion-controlled reaction one might have to differentiate between diffusion of ions through the pore water in the gel and diffusion of ions through a solid mass, or consider a mixture of these two possible mechanisms. For these two diffusion mechanisms a different temperature sensitivity may hold. Since the boundary and diffusion mechanisms can occur simultaneously, it is obvious that the temperature dependency of the reaction processes as observed on macro-scale is, in fact, the "net" result of the temperature dependency of individual processes and mechanisms. Parameters with which the temperature dependency is generally described must therefore be indicated as "apparent quantities".
In HYMOSTRUC the effect of temperature on the rate of reaction has been allowed for with two temperature function $F_1(\cdot)$ and $F_2(\cdot)$. The first one refers to the effect of the temperature on the rate of processes and mechanisms involved in the hydration process. The second one allows for the effect of temperature-induced changes in the morphology and microstructure of the reaction products.

Net Temperature Effect
The effect of temperature on the rate of physical and chemical phenomena is accounted for with the function $F_1(\cdot)$, which is based on the Arrhenius function:

$$F_1\{T, \alpha, C_3S\} = A * e^{-\frac{E \cdot \{T, \alpha, C_3S\}}{R*(273+T)}} \tag{3.25}$$

in which R is the gas constant (8.31 J/mol °K) and E the apparent activation Energy. The latter quantity was found to be function of the actual values of the degree of hydration α, the curing temperature T and the chemical composition, c.q. the C_3S content, of the cement [4]. In formula form:

$$E\{T, \alpha, C_3S\} = p_0 * \alpha * e^{-[m*(C_3S\%)^n + 0.025*T^{3/2}]} + 0.33 * (C_3S\%) + 30 \tag{3.26}$$

with $m = 2.52 \ 10^{-11}$ and $n = 6.15$ [4]. For the constant A in equation (3.25) it holds:

$$A = e^{\frac{E(T_{20})}{R*293}} \tag{3.27}$$

in which $E(T_{20})$ is the apparent activation energy for $T = 20\,°C$.
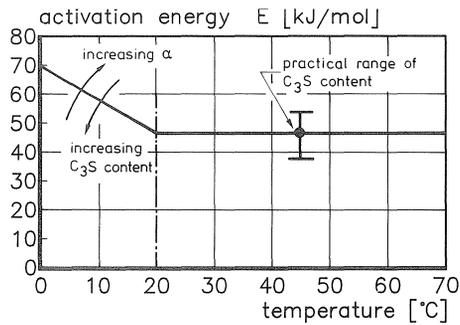
Fig. 3.14   Apparent activation energy as function of reaction temperature [4].

In Fig. 3.14 the apparent activation energy is expressed as a function of the reaction temperature. The influence of the C_3S content and of the degree of hydration is indicated qualitatively.

Morphology and Structure Related Temperature Effects

To allow for the effect of densification of hydration products due to *high reaction temperatures* on the rate of hydration a temperature function $F_2(\cdot)$ is introduced. From an evaluation of experimental data on the relationship between capillary porosity and curing temperature, whereby the increase in capillary porosity with increasing temperature has been ascribed to densification of the hydration products, the following expression for the temperature dependency of the density of hydration products has been derived (for $0 < T < 60\,°C$) [4]:

$$\nu(T) = 2.22 * e^{-28 \ 10^{-6}*T^2} \tag{3.28}$$

In this expression the temperature T refers, in essence, to an isothermal temperature regime. In case of a variable curing temperature, as is the normal case in engineering practice, a "weighted temperature $\bar{T}$", i.e. the mean temperature in the *hydration domain,* is adopted according to:

34

$$\bar{T}_j = \frac{1}{\alpha_j} * \int_0^{\alpha_j} T(\alpha)\, \mathrm{d}(\alpha) \tag{3.29}$$

It is assumed that temperature-caused densification of the diffusion layer allows for a reduction of the rate of penetration of the reaction front according to:

$$F_2(\bar{T}) = \left(\frac{\nu(\bar{T})}{\nu_{20}} \right)^{\beta_2} \tag{3.30}$$

in which $\nu_{20} = \nu(T_{20})$ and β_2 is a factor to be determined from an evaluation of adequate experimental data.

The temperature dependency of the density of the hydration products will *also* affect the magnitude of the transition thickness $\delta_{tr}(\cdot)$. Temperature-induced densification of the products layer is assumed to cause a reduction of the transition thickness according to:

$$\delta_{tr}(\bar{T}) = \delta_{tr,20} * \left(\frac{\nu(\bar{T})}{\nu_{20}} \right)^{\beta_2} \tag{3.31}$$

in which $\delta_{tr,20}$ is the transition thickness for isothermal hydration at $T = 20\,^\circ\mathrm{C}$. For mathematical evaluations in view of implementation of the expressions (3.28) to (3.31) in equations (3.20a, b) reference is made to [4]. For the Basic Rate Equation we finally get:

$$\frac{\Delta \delta_{in;x,j+1}}{\Delta t_{j+1}} = K_0 * F_1(\cdot) * \Omega_1(\cdot) * \Omega_2(\cdot) * \Omega_3(\cdot) * \left[\left(\frac{\nu(\bar{T}_j)}{\nu_{tr}(\bar{T}_j)} \right)^{\beta_2} * \left\{ \left(\frac{\nu(\bar{T}_j)}{\nu_{20}} \right)^{\beta_2} * \frac{\delta_{tr,20}}{\delta_{x,j}} \right\}^{\beta_1} \right]^{\lambda} \tag{3.32}$$

With the basic rate formula (3.20), i.e. eq. (3.32), the rate of penetration of the reaction front in a cement particle with diameter x can be determined. From the penetration depth the amount of cement that has reacted can be computed. The overall degree of hydration of a poly-size sample is found by adding the amounts of the cement of all the cement particles in the system.

In the basic rate formula (3.32) the effect of the particle size distribution, the w/c factor and the temperature are allowed for explicitly. The effect of the chemical composition of the cement on the rate of penetration was not considered yet. The model parameters $K_0 = K_0(\cdot)$, $\delta_{tr,20} = \delta_{tr}(\cdot)$, β_1 and β_2, which have to be determined yet, were expected to exhibit dependence on the chemical composition of the cement.

3.4.3 Chemical Composition of the Cement. Independent Model Parameters

3.4.3.1 General

In the foregoing sections the effect of particle interaction, the state of water and temperature on the rate of hydration of individual cement particles have been considered. Explicit modelling of the effect of these parameters on the rate of penetration of a reaction front into a cement particle has resulted in a basic rate formula, in which four parameters, i.e. *Independent Model Parameters,* have still to be determined.

From theoretical point of view it is to be expected that the basic rate factor $K_0(\cdot)$ and the transition thickness $\delta_{tr}(\cdot)$ will exhibit a dependence on the chemical composition of the cement. To verify the expected correlation an extensive evaluation program has been carried out in which the four model parameters a parameters, viz. $K_0(\cdot)$, $\delta_{tr}(\cdot)$, β_1 and β_2, where determined [4]. In this program over 60 hydration tests were involved, comprising 27 different types of cement with C_3S contents ranging from 15% to 70%. The w/c ratios varied from 0.16 to 0.8, particle size distributions with n-values (equation (3.4)) ranging from 0.73 to 3.15 and curing temperatures from 4 °C up to over 50 °C. The model parameters were determined so as to achieve a satisfactory fit of the experimental data.
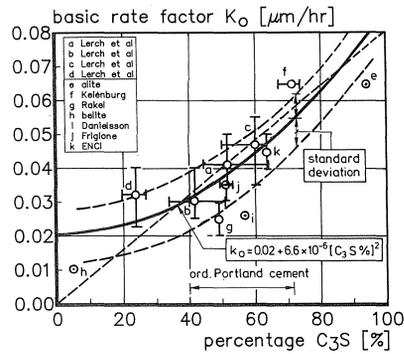
Fig. 3.15   Basic rate factor $K_0(\cdot)$ as a function of the C_3S content of the cement.
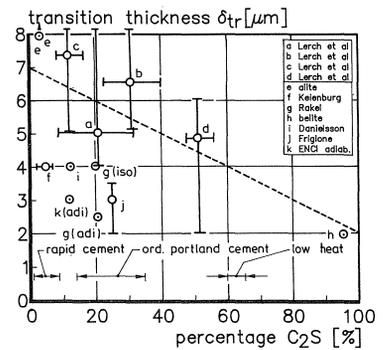
Fig. 3.16   Transition thickness $\delta_{tr}(\cdot)$ as a function of the C_2S content of the cement.

3.4.3.2   Basic Rate Factor K_0

Mathematical Expression for K_0

The evaluation program revealed a distinct correlation between the K_0-values and the C_3S content of the cement. The higher the C_3S content, the higher the K_0-values. Results are shown in Fig. 3.15. The figure shows that, although the correlation is obvious, the scatter is quite substantial.

For this correlation a parabolic expression holds quite well. A linear correlation, however, would not be bad either. For the parabolic correlation it holds that:

$$K_0 = 0.02 + 6.6 \ 10^{-6} * [C_3S\%]^2 \quad [\mu m/h] \tag{3.33}$$

For C_3S-contents in ordinary Portland cements in the range from 30% up to 70% [4] expression (3.33) holds quite well. For the standard deviation $s(K_0)$ a value of $s = 0.008$ $\mu m/h$ was obtained. It was found that this standard deviation could be carried back to quite a substantial extent to the inaccuracies in the chemical composition, i.e. the C_3S content, which we have to consider [4]. In addition to the effect of variations in the C_3S content which appear to contribute to the scatter in the K_0-values one should consider

36

effects of minor compounds and gypsum, which effects have not been accounted for explicitly in HYMOSTRUC.

It is noticed, that the basic rate factor is the *only* model parameter which influences the rate of reaction in the early boundary reaction stage of the hydration process. Hence, its value is not affected by the values of the three remaining model parameters which become operational no sooner than in the diffusion controlled stage of the process (equation (3.20), when $\lambda = 1$).

3.4.3.3 Transition Thickness δ_{tr}

Fig. 3.16 shows the transition thickness δ_{tr} as a function of the C_2S content determined in the evaluation program. The δ_{tr}-C_2S correlation is evidently less distinct than the K_0-C_3S correlation. For the data of Lerch et al. and the alite and belite data a linear decrease of the transition thickness with increasing C_2S content seems to hold. The δ_{tr}-values found from the evaluation of the test data of Frigione, Rakel, Danielsson, Keienburg and the ENCI tests, however, are substantially lower. The only guidance that can be deduced from Fig. 3.16 is that for the majority of ordinary Portland cements the transition thickness varies between 2.5 μm and 6.0 μm. For low-heat cements the transition thickness turns out to be relatively low, whereas for rapid hardening cements the best results are yielded with relatively high values of the transition thickness. Computer simulations could start with the guide values for δ_{tr} according to:

$$\delta_{tr} = -0.02 * [C_2S\%] + 4 \quad [\mu m] \tag{3.34}$$

With respect to the large scatter in the δ_{tr}-values it is noticed that this does not necessarily jeopardize the applicability of HYMOSTRUC for practical purposes [4].

3.4.3.4 Coefficients β_1 and β_2. Guide Values

For the absolute values of the β-coefficients it can tentatively be stated that:
1. The majority of test results could be approximated satisfactorily for $\beta_1 = 2$ and $\beta_2 = 2$.
2. As the hydration process progresses the β_2-values tend to increase.

Variations in the β-values in the range from 1 to 2 could cause variations in the predicted 28-days hydration values of about 5% to 10%. Variations of the same order of magnitude can be ascribed to variations in the gypsum content and the effect of minor compounds [4]. Since the effects of gypsum and minor constituents are not accounted for explicitly in the model yet, attempts to correlate the β-values to the chemical composition of the cement are not warranted.

3.4.3.5 Default Values of Model Parameters

When used for practical purposes HYMOSTRUC operates with the *default values* for the independent model parameters according to equations (3.33) and (3.34) and

37

$\beta_1 = \beta_2 = 2$. When applied for research purposes, i.e. when the values of the independent model parameters have to be established, the model parameters can be inserted manually so as to obtain the best possible fit of theoretical and experimental data. In the latter case the default values of the model parameters can be used as starting values for the iteratively determined final values.

3.4.3.6 General Remarks in view of Consistency of the Model

From the very outset of the evaluation programm it was assumed that the β-coefficients might exhibit a dependency on the chemical composition of the cement. The evaluation programm, however, did not reveal such a dependency. Moreover, although the variation in β-values varied from 1 to 2, the effect on the shape of the predicted hydration curves was relatively small [4]. It this respect it is considered worthwhile to note, that the β-coefficients become operative no sooner than in the diffusion controlled stage, i.e. when the degree of hydration has reached a value between $\alpha = 0.3$ to 0.5 already. Until these α-values the shape of the hydration curve is determined (at least in the model) by the paste parameters like w/c ratio, the particle size distribution of the cement, the reaction temperature and, as far as the independent model parameters are concerned, *only* by the basic rate factor K_0. Beyond aforementioned α-values, i.e. in the stage when the degree of hydration increases up to about 0.6 to 0.8, variations in the β-values from 1 to 2 will generally cause variations in the predicted 28-day hydration values of about 5% to 10%. Variation of the same order of magnitude can be ascribed to variations in the gypsum content and the effect of minor compounds [4], which effects are not modelled explicitly in HYMOSTRUC. In the light of the latter fact it must be considered fruitless to search for a correlation between the β-values and the chemical composition of the cement unless we would be able to account for the effect of minor compounds and gypsum explicitly in the model (see also Section 3.4.3.4).

For a more detailed discussion as regards the consistency of the set of independent model parameters and the reliability of the model, reference is made the original report [4].

4 Characteristics and Simulation Potential of HYMOSTRUC

4.1 *Introduction*

With the simulation program HYMOSTRUC hydration curves of Portland cement-based systems can be calculated as a function of the chemical composition and particle size distribution of the cement, the w/c ratio and the reaction temperature. Microstructural development, i.e. the formation of interparticle contacts, is quantified explicitly as well as its effect on the rate of hydration. It is particularly the allowance for microstructural development which distinguishes the model from earlier proposed models and which aspect shall, therefore, be addressed in more detail in this chapter.

4.2 Modelling of Microstructural Phenomena

4.2.1 Clustering of Particles in the Early Stage of Hydration

When the hydration process proceeds, small particles will become embedded in the outer shell of larger particle. Consequently the number of small *free particles or free clusters,* i.e. particles and clusters of particles which are not embedded in the outer shell of larger particles, will decrease, whereas the number of large particles or large clusters must increase. A shift from a large number of small particles to a smaller number of large particles has been observed by Odler et al. [78] (Fig. 4.1). Results, which refer to an ordinary Portland cement paste, $\omega_0 = 0.3$ and Blaine $= 300$ m^2/kg, are presented in Fig. 4.2 with dashed curves. The solid curves show the same trend as found with HYMOSTRUC, beit for a paste with w/c ratio $\omega_0 = 0.5$. A comparison of results is nevertheless judged warranted as in the early stage of hardening the influence of the w/c ratio is note very significant as far as the phenomenon in view is concerned. Taking into account, on the one hand, the experimental difficulties and experimental error with counting the number of particles in a hydrating mass and, on the other hand, the simplifications carried through in HYMOSTRUC, it can be concluded that the experimental and theoretical data are in good agreement with each other. This warrants the conclusion that the concept of embedding small particles in the outer shell of larger ones as considered and modelled in HYMOSTRUC is not in contradiction with experimental results.
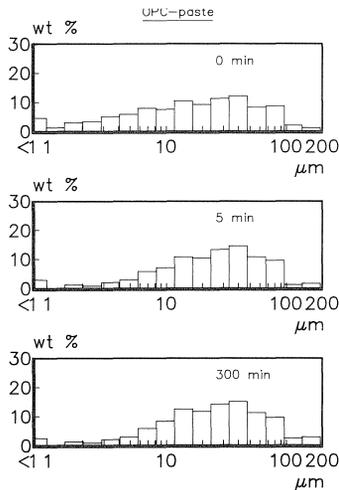
Fig. 4.1 Changes in particle size distribution in a hydrating paste observed by Odler et al. [78].
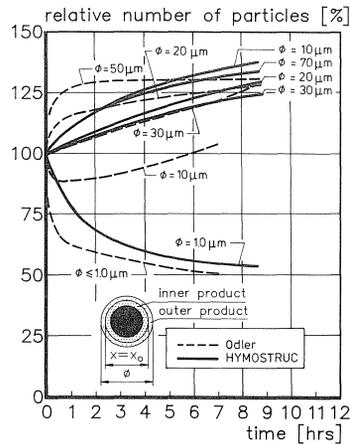
Fig. 4.2 Proportional changes in particle size distribution in a hydrating paste. Experimental: Odler [78].

4.2.2 Embedding of Particles and Shell Expansion

For a cement paste made with cement of moderate fineness (Blaine ≈ 320 m^2/kg), $\omega_0 = 0.5$, Fig. 4.3 shows the amount of cement embedded in the outer shell of particles

with diameters $x = 2, 4, 8, 16, 32$ and 64 µm as a function of time. The embedded cement in the outer shell of large particles can result in a significant increase of the thickness of the outer shell. This is illustrated in Fig. 4.4, where the increase of the shell thickness is shown as a function of the particle diameter at various times. It appears that during the first 50 hours of the hydration process the effect of the particle size on shell growth is not very significant. At later stages, however, when the amount of embedded cement in the outer shell further increases, the shell thickness increases significantly. This increase is greater the larger the particle diameter.

It is to be expected that particularly for large particles the extra growth of the shell due to particle embedding will significantly affect the rate of hydration. Ignoring the extra increase of the effective thickness of the diffusion layer will result in misinterpretations with respect to the hydration mechanisms which might have occurred at different stages of the hydration process and hence to incorrect values of rate parameters such as diffusion coefficients.
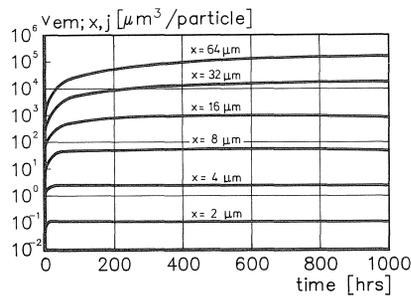
Fig. 4.3   Embedded cement volume $v_{em;x,j}$ in outer shells of hydrating particles. Paste: $\omega_0 = 0.5$, Blaine ≈ 320 m^2/kg.
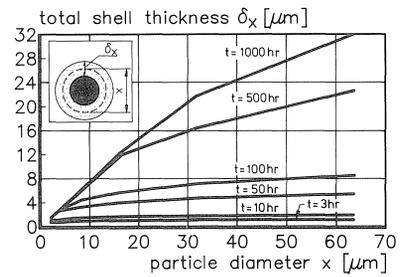
Fig. 4.4   Shell thickness δ_x as a function in outer shells of hydrating particles. Paste: $\omega_0 = 0.5$, Blaine ≈ 320 m^2/kg.

4.3   *Factors Affecting the Rate of Hydration*

4.3.1   Effect of Particle Interaction on Rate of Penetration of the Reaction Front

Initial Rate of Penetration

The initial rate of penetration of the reaction front is given with the basic rate factor $K_0(C_3S)$ [µm/h] and is, at first, the same for all particle diameters. For a large number of cements the $K_0(C_3S)$-values were found to range from 0.02 µm/h for a *low C_3S – high C_2S* cement to 0.07 µm/h for a *high C_3S – low C_2S* cement.

Comparison of K_0-Values with Literature Data

Several authors have presented values for the rate of penetration of the reaction front in hydrating cement particles. In so far these values refer to the early stage of the reaction process, i.e. the stage when the boundary reaction is the rate-controlling

40

mechanism, these values can be compared with the K_0-values. Early penetration rate data is shown in Table 4.1. It is noticed that the data of this Table do not merely reflect a materials property but also are they a function of the measuring method used to obtain the data. This means, that caution should be exercised when comparing these data with the K_0-values of Fig. 3.15. However, it can be concluded that the range of published penetration rates agrees with the K_0-values found in the evaluation program in this chapter. The penetration rates for alite and C_2S determined by Tsumura [17] correspond fairly well to the K_0-value for alite and belite (Compare also Fig. 3.15, points e and h).

Table 4.1 Rate of penetration of the reaction front in cement particles and compounds (Temperature: $\pm 20°C$)

author	ref.	year	reference period	material	penetration rate $\mu m/h$
Anderegg et al.	[7]	1929	0–24 h	cement	0.02
Krogbeumker	[81]	1972	0–72 h	Portland cement	0.032
Steinherz	[83]	1960	0–72 h	cement cliner	0.021
Tsumura	[17]	1966	first hrs	alite	0.055
			first hrs	C_3S	0.036
			first hrs	C_2S	0.0011
Lhopitallier et al.	[82]	1948	1st mnth	cement clinker	0.042
Taplin	[55]	1968	>1000 h	alite	0.0125
				β-C_2S	0.0009
Bezjak	[80]	1980	phase-bound	alite	0.067
			phase-bound	comm. cement	0.074–0.110

Evolution of the Rate of Penetration

When hydration proceeds, the rate of penetration will decrease due to the effect of different reduction mechanisms as discussed in [4]. For a paste with w/c ratio $\omega_0 = 0.65$ the rate of of penetration of particles $x = 4, 8, 16$ and 64 μm is shown in Fig. 4.5. Since, due to embedding of small particles, the expansion of larger particles exceeds that of small particles, the former will reach the diffusion controlled stage sooner than the latter. Moreover, the water withdrawal mechanism will affect the rate of penetration of the larger particles more than the small particles. Consequently, the rate of penetration at an arbitrary point of time will differ for different particle sizes. For low w/c ratios the rate of penetration of larger particles may tend to zero while at the same time smaller particles may still continue to hydrate.

4.3.2 Effect of Particle Interaction on Overall Rate of Hydration

As explained in Section 3.4.2.2 the effect of embedding small particles in the outer shell of larger particles is two-fold. Firstly, as shown in the foregoing, the embedding of particles causes an extra expansion of the large central particles, which will result in an extra diffusion resistance of the product layer.

41

Secondly, embedded but still hydrating particles will withdraw water from the central particle in the outer shell of which they are embedded. The effects of these two aspects are illustrated in Fig. 4.6. For a cement paste with $\omega_0 = 0.4$, made of a cement with moderate fineness, three simulations where carried out. In the first simulation, represented by curve I, no extra expansion caused by embedding of particles and water withdrawal was considered. Curve II refers to a simulation in which extra expansion due to embedding of particles was taken into account indeed, whereas curve III reflects the effect of both extra particle expansion and water withdrawal.
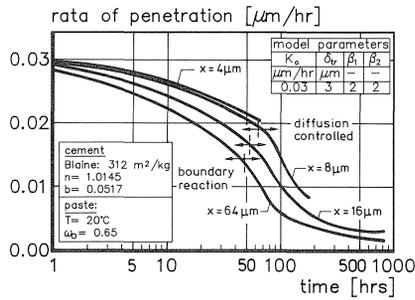
Fig. 4.5 Rate of penetration of the reaction front as a function of time for different particle sizes [4].
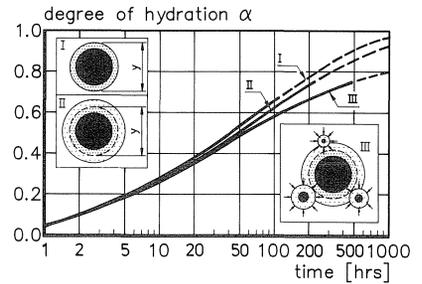
Fig. 4.6 Effect of extra particle expansion and water withdrawal mechanism on overall rate of hydration [4].

To illustrate the effect of the two rate reducing factors as clear as possible the simulations have been carried out with arbitrary values of the basic rate factor $K_0(C_3S)$ and have been extended beyond a practical ultimate degree of hydration of about 0.7. For this value of the degree of hydration ignorance of extra particle expansion and water withdrawal reveals to cause a difference in the calculated degree of hydration of about 15%. Although this 15 percent is a *model-bound* value and can, therefore, only give an *indication* of the effect of particle interaction on the rate of hydration, it seems justified to concluded that ignorance of the effect of particle interaction will almost inevitable lead to misinterpretations of test results as regards hydration mechanisms and rate constants, c.q. diffusion coefficients.

4.4 *Simulation Potential of HYMOSTRUC*

To illustrate the potential of the simulation model to describe the effects of individual paste parameters like the particle size distribution of the cement, w/c ratio and the temperature some examples will be presented. The examples are taken from the evaluation program mentioned in Section 3.4.3. For a complete description of the examples reference is made to [4].

42

4.4.1 Effect of Particle Size Distribution

To check the potential of HYMOSTRUC to simulate the effect of the particle size distribution on the rate of hydration correctly, experimental data of Keienburg [84] has been used. For three different types of cement Keienburg investigated the effect of the cement fineness on the rate of hydration and strength development. Hydration data was obtained from mortar samples, manufactured with $\omega_0 = 0.5$ and cured at 20 °C under saturated conditions. The degree of hydration was obtained by dividing the measured non-evaporable water content by the maximum amount of chemically bound water calculated on the basis of the Bogue composition of the cement.

For a coarse, moderate and fine sample of each of the three cements the results of the mathematical analyses are shown in Fig. 4.7. In the legends some sample data is given as well as the model parameters of HYMOSTRUC for which a good approximation of the experimental data was possible. It appears that a satisfactory approximation of the experimental data is possible with only one set of model parameters. Obviously, and in line with what was expected, the model parameters are independent of the particle size distribution of the cement.

degree of hydration α

No.	C_3S	C_2S	C_3A	C_4AF
● A	73.2	8.1	7.0	8.7
× B	74.2	3.3	10.1	10.2
○ C	67.7	6.4	9.9	11.2

Blaine	coarse	fine
● A	199	514m²/kg
× B	198	507m²/kg
○ C	208	502m²/kg

wcr = 0.5
temp. = 20℃

calculations:
A ———
B — —
C ----

model parameters			
K_0	δ_{tr}	β_1	β_2
$\mu m/hr$	μm	—	—
0.065	4.0	1	1

degree of hydration α

No.	C_3S	C_2S	C_3A	C_4AF
● A	73.2	8.1	7.0	8.7
× B	74.2	3.3	10.1	10.2
○ C	67.7	6.4	9.9	11.2

Blaine	intermediate
● A	356m²/kg
× B	353m²/kg
○ C	349m²/kg

wcr = 0.5
temp. = 20℃

calculations:
A ———
B — —
C ----

model parameters			
K_0	δ_{tr}	β_1	β_2
$\mu m/hr$	μm	—	—
0.065	4.0	1	1

a. Fine and coarse cements   b. Cement of Moderate fineness

Fig. 4.7   Effect of cement fineness on the rate of hydration in mortar. Sealed curing.
      – Experimental hydration data (Keienburg [84]): indicated with vertical bars.
      – Approximations with HYMOSTRUC presented with solid curves.

It is worthwhile to notice that, although the chemical composition of the three cements does not vary significantly, the hydration data does exhibit quite a scatter. In the present stage of development of the model the effect of the chemical composition on the course of the hydration process is only poorly dealt with. Better result can only be expected if all chemistry-related aspects, including the effects of minor components and gypsum, are modelled explicitly [4].

It is noticed that the K_0-value is relatively high and the δ_{tr}-value relatively low as compared with the default values mentioned in Section 3.4.3. A high value of K_0 implies a relatively high degree of hydration. Also Keienburg has pointed to the high degrees of hydration in his tests. After an evaluation of his tests he concluded, however, that there was little scope to doubt the measurements. Bearing in mind that in Keienburg's tests

hydration of the mortar samples took place under saturated conditions, which must have resulted in higher hydration values, and that, moreover, hydration in mortar is said to proceed more rapidly than in neat pastes, the relatively high degree of hydration in these tests seems to be partly explained.

4.4.2 Effect of Water/Cement Ratio

In Fig. 4.8 heat of hydration data (conduction calorimetry) reported by Danielsson [85] is given. This data refers to sealed cement pastes, manufactured with w/c ratios ranging from 0.25 to 0.5. The degree of hydration was obtained by dividing the measured heat of hydration by the calculated maximum heat of hydration liberated at complete hydration. The cement characteristics are also included. Since no information was provided on the particle size distribution, the R-R coefficients were taken to obtain the given Blaine surface of 312 m^2/kg. With the thus obtained particle size distribution the degree of hydration was calculated and compared with the measured degree of hydration (Fig. 4.9). The experimental data, indicated with discrete points, could be approximated satisfactorily with model parameters as indicated in Fig. 4.9.
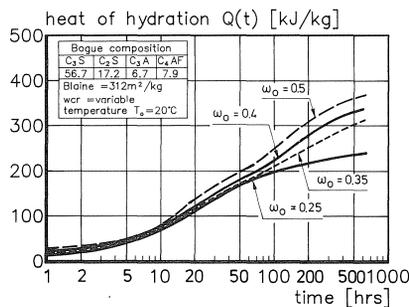
Fig. 4.8 Heat of hydration of neat pastes. Sealed curing; Danielsson [85].
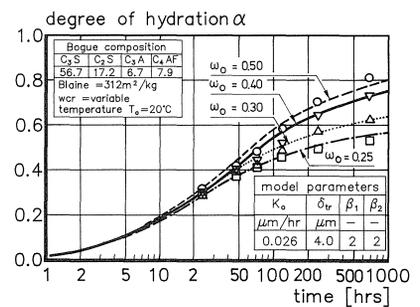
Fig. 4.9 Measured and approximated degree of hydration. Test of Danielsson 85].

4.4.3 Effect of Temperature

To check the ability of HYMOSTRUC to simulate the effect of temperature on the rate of hydration both isothermal and adiabatic test data have been analyzed. The isothermal test data is the classical data of Lerch and Ford [86]. For the adiabatic test data we have chosen that published by Laube [87] and Rakel [88].

4.4.3.1 Isothermal Tests of Lerch and Ford

In their excellently documented "Long-time Studies" Lerch and Ford [86] have described the hydration data of Type I, II, III and IV cement at different temperature levels. Mean values of the fineness (Blaine) and of the fineness parameters n and b (Rosin-Rammler) of these cements as deduced from the original paper are indicated in

44

Table 4.2. Mean values of the C_3S content are indicated in this table as well. Curing occurred under sealed conditions at temperatures 4.4 °C, 23.9 °C, 32.2 °C and 40.4 °C. Similarly to the averaging of the cement characteristics, the experimentally obtained hydration data of the cements belonging to a certain cement type was averaged out yielding average hydration data for each type of cement. The mean hydration values for the Type II and Type III cements are shown in Fig. 4.10a, b with discrete points. For cement Type III vertical bars indicate the range of hydration values observed for the individual cements.

Simulations carried out with HYMOSTRUC are indicated with solid lines. The results are obtained with the average values of the model parameters K_0 and δ_{tr} indicated in the legends of the figures. These values where obtained from an evaluation of hydration data obtained at 21 °C [4]. From the comparison of the average of the measured hydration curves and the predictions with HYMOSTRUC it is evident that the thus obtained model parameters hold excellently also at temperatures different from 21 °C.

Table 4.2 Characteristics of fictitious cements Type I, II, III, and IV [4, 86]

type of cement	number of samples	fineness [m²/kg]	PSO		C_3S [%]
			n	b	
I	7	372	0.978	0.0382	51.4
II	4	314	1.003	0.0288	41.6
III	3	564	1.021	0.0620	60.0
IV	3	360	1.031	0.0362	24.0

As regards the widths of the scatter in the experimental data, note that this scatter must result from (relatively small) differences in the cement composition. Particularly differences in the alkali content of individual cements might have resulted in a substantial scatter of the hydration data.


a. Type II cement b. Type III cement
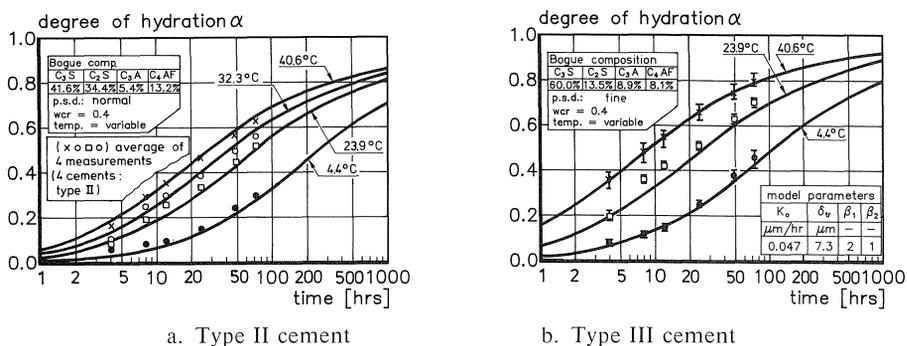
Fig. 4.10 Effect of curing temperature on rate of hydration, measured (discrete) and theoretical values (solid lines). Hydration data refer to Type II and III cement, published by Lerch et al. [86].

45

4.4.3.2 Adiabatic Hydration Tests

Effect of Initial Concrete Temperature on Adiabatic Hydration Curves

Fig. 4.11 shows the effect of the initial concrete temperature on the rate of hydration. The temperature curves refer to a concrete with a cement content of 240 kg/m^3 and 80 kg/m^3 fly-ash.
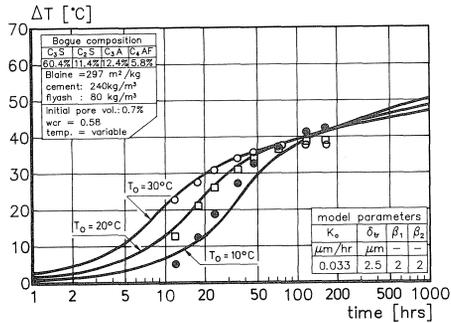
Fig. 4.11 Adiabatic temperature rise as a function of time for different initial curing temperatures. Data of Laube [87].
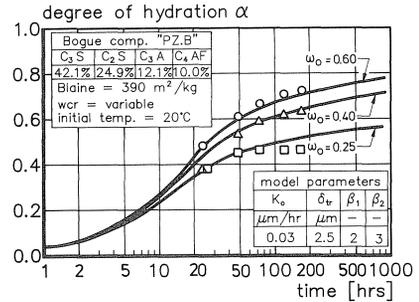
Fig. 4.12 Adiabatic hydration curves. Portland cement. W/C ratio ω_0 variable. Test data of Rakel [88].

In the calculations, of which the results are shown in Fig. 4.11 with solid lines, the temperature dependency of the specific heat was taken into account according to [89]. The fly-ash was considered to behave as an inert filler during the first 28 days of hydration. This is, of course, a simplification of reality, and thus the calculations must be considered as indicative only. The calculated temperature curves are nevertheless interesting, since they reveal, in agreement with the measured temperatures, a higher temperature rise in the case of lower initial temperatures of the mix. This phenomenon is to be attributed to the lower specific heat of the concrete at lower temperatures and the temperature-related changes in the morphology, i.e. density and hence diffusion resistance of the hydration products [4].

It is further commented that the flat slope of the measured hydration curves for curing times exceeding $\approx$ 3 days is hard to simulate with HYMOSTRUC unless the value of β_2 is significantly increased. A physical background for such an increase might be sought in an higher density of the hydration products when formed at high temperatures.

Effect of Water/Cement Ratio on Adiabatic Hydration Curves. Experiments by Rakel

In Fig. 4.12 adiabatic tests are presented carried out by Rakel [88]. The w/c ratio varied from 0.25 to 0.6. The effect of the w/c ratio on the rate of hydration is predicted fairly satisfactory with HYMOSTRUC.

46

4.5 Strength Development

4.5.1 Embedded Centre Plane Area and Strength

4.5.1.1 Effectiveness of Individual Particle Fractions as Regards Strength Development

In Fig. 4.13 the embedded contact area $\Delta A_{em;x}$ per fraction is shown as a function of the particle size. Only the embedded contact areas of the free particles in the fractions are considered. Time is inserted as a parameter. The figure shows that with elapse of time the major contributions to the contact area subsequently come from fractions with higher particle diameters. Over a long period of time, i.e. from 50 to 1,000 hrs, the major contributions to the embedded centre-plane area come from the fractions between 10 and 30 μm. This finding is in good agreement with the results published by many authors, who also found that the fractions between 10 and 30 μm are of major importance in view of strength development (see [4]).

The large particles hardly contribute to the centre-plane area in the early stage of the hydration process, whereas at later stages they do. This is considered to be in agreement with the observation that the ultimate strength benefits from the presence of large particles [4].

4.5.1.2 Embedded Centre Plane Area versus Strength. Effect of W/C Ratio

In Section 3.3.4.2 it has been suggested already, that the embedded cement volume and the embedded centre plane area might exhibit a correlation with the strength. In this
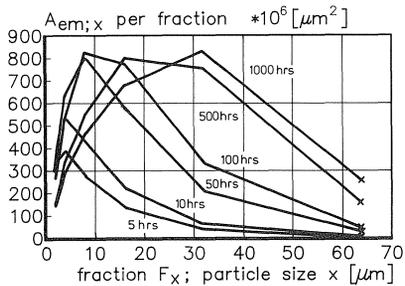

Fig. 4.13 Embedded centre-plane area $\Delta A_{em;x}$ per fraction as a function of the particle size. $\omega_0 = 0.5$ [4].
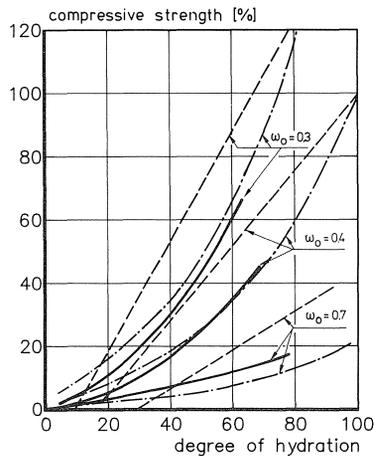
Fig. 4.14 Relative increase in strength and embedded centre-plane area [4].

47

section we restrict ourself to the relationship between embedded centre plane area and strength. In order to check the reasonableness of the assumed correlation the proportional increase in the summarized embedded centre-plane area is compared with the proportional increase in strength as deduced from experimental data published by Powers [91] and Fagerlund [92]. These proportional increases are shown in Fig. 4.14 as a function of the degree of hydration for pastes with w/c ratios 0.3, 0.4 and 0.7. The observed relatively good agreement between the three sets of curves suggest, as expected, a good correlation between strength and the amount of embedded cement.

4.5.2 Interparticle versus Transparticle Fracturing

An interesting feature of HYMOSTRUC in view of strength considerations is the option to quantify the physical interaction between expanding particles. From literature it is well known, that with progress of the hydration process the fracture mode changes from interparticle to transparticle. Both fracture modes are shown diagrammatically in Fig. 4.15. Obviously there is a moment, i.e. a degree of hydration, beyond which the strength of the contact points and contact surfaces between adjacent particles exceeds the strength of the shell of hydration products that surrounds the anhydrous core of a cement grain. For a particle x this moment is determined by the ratio between the surface area $AR_{x,\alpha}$ of a ring with outer radius $R_{ou;x,\alpha}$ and thickness $\delta_{x,\alpha}$ viz. (see Fig. 4.16):

$$AR_{x;\alpha} = \pi * \left[R_{ou;x,\alpha}^2 - (R_{ou;x,\alpha} - \delta_{x;\alpha})^2 \right] \tag{4.1}$$

on the one hand, and 50% of the total embedded centre-plane area of the particle considered, on the other. With regard to the embedded centre-plane area it seems plausible to assume that those particles which are most effective in interparticle load transfer are those of which the diameter exceeds the thickness of the outer shell of a central particle. The centre-plane area that remains after subtraction of the contribution of the embedded particles with diameters smaller than the outer shell thickness is called the
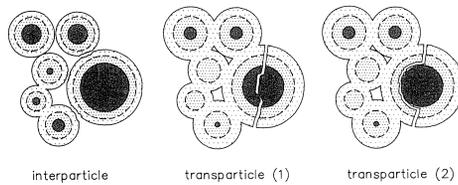
Interparticle fracturing   Transparticle fracturing

Fig. 4.15 Interparticle versus transparticle facture mode (schematic representation).
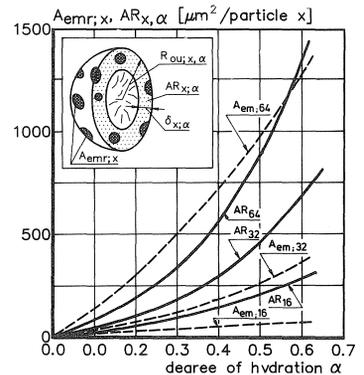
Fig. 4.16 Reduced embedded centre-plane area $A_{emr,\alpha}$ versus ring area $AR_{x;\alpha}$ of the central particles.

48

"reduced embedded centre-plane area $A_{emr;x}$". For several particle sizes the ring area $AR_{x,a}$ and the reduced embedded centre-plane area are shown in Fig. 4.16 as a function of the overall degree of hydration. It turns out that for small particles the ring area always exceeds the reduced embedded centre-plane area. For large particles the reduced embedded centre-plane area approaches or can even exceed the ring area of the shell which surrounds the anhydrous core. These particles are considered to be susceptible to the transparticle fracture mode.

4.5.3   Embedded Cement Volume and Strength Development

4.5.3.1   Effect of Water/Cement Ratio

Just like the embedded centre-plane area the embedded cement volume, i.e. the amount of cement involved in interparticle interactions, is expected to be a possible strength parameter. For pastes with w/c ratios $\omega_0 = 0.4$ and $\omega_0 = 0.5$, *absolute* values of the measured compressive strength are presented as a function of the calculated degree of hydration and the calculated amount of embedded cement per μm^3 paste in Fig. 4.17. Whereas the relationship between strength and degree of hydration still exhibits a pronounced dependence on the w/c ratio (Fig. 4.17a), the relationship between strength and embedded cement volume reveals to be almost independent of the w/c ratio (Fig. 4.17b). This information tends to confirm the assumption that strength is correlated with the number of interparticle contacts, provided we may state that the amount of embedded cement is a measure for the number of interparticle contacts.

a. Strength vs. degree of hydration   b. Strength vs. embedded cement volume
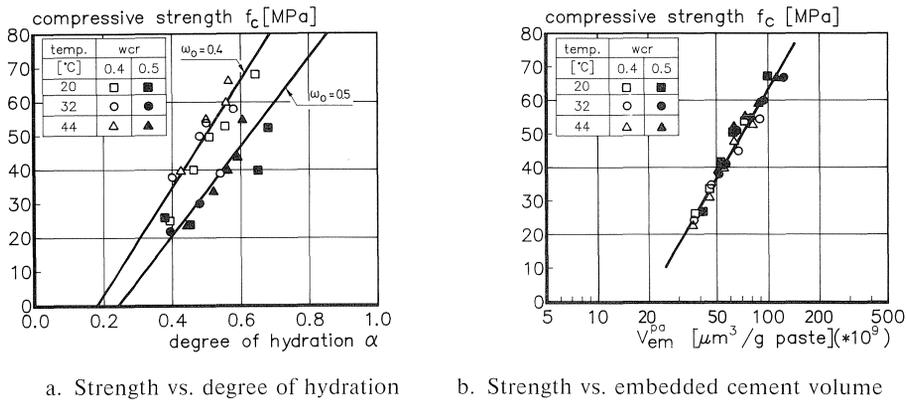
Fig. 4.17   Strength of mortar as a function of the degree of hydration (Fig. 4.17a) and the amount of embedded cement v_{em}^{pa} [2] (Fig. 4.17b).

4.5.3.2   Simulation of the Effect of Temperature

The reasonableness of the assumed correlation between strength and embedded cement volume receives further support from an evaluation of the effect of the curing temperature on strength development. As noticed in Section 3.4.2.4 already, higher

temperatures would cause a reduction of the ν-factor, i.e. the quotient of the volume of the gel and the reactant. A smaller ν-factor at elevated temperatures causes less expansion of hydrating particles and hence a reduction of the amount of embedded cement, of the number of the interparticle contacts and, consequently, of the strength. The data presented in Table 4.3 seems to confirm the foregoing reasoning. The 28-days strengths of pastes, $f_{c,28}(T)$, cured at $T = 22, 30, 40$ and $50\,°C$, respectively, is presented together with the calculated amount of embedded cement $v_{em,28}(T)$. The decrease in strength with increasing temperatures turns out to correlate quite well with the decrease in the amount of embedded cement. From the foregoing it seems justified to consider the amount of embedded cement as a rather solid strength parameter with a high potential to explain strength development on a microstructural basis.

Table 4.3 Effect of curing temperature on compressive strength of pastes and embedded cement volume after 28 days hydration.

curing temperature	degree of hydration	compressive strength at 28 days (measured)		embedded cement volume $v_{em,28}$ at $\alpha_{t=28}$ (calculated)	
T [°C]	(measured) $\alpha_{t=28}$	$f_{c,28}(T)$ [MPa]	$f_{c,28}(T)/f_{c,28}$ (22 °C) relative	$v_{em,28}(T)$ [μm^3/g cement]	$v_{em,28}(T)$ß$v_{em,28}$ (22 °C) relative
22	0.730	60.8	100%	145 10^9	100%
30	0.734	53.4	88%	142 10^9	98%
40	0.734	51.3	84%	134 10^9	92%
50	0.754	48.5	80%	123 10^9	85%

4.5.4 Matrix-Aggregate Interfacial Zone

Since HYMOSTRUC accounts for the stereological aspect of microstructural development explicitly, evaluation of the effect of the *packing of particles* in the interfacial zone on the porosity of the paste in this zone is possible. Going from the surface of an aggregate particle in outward direction the amount of cement found in a shell around this particle, in other words the *local paste density* $\zeta^L(y)$, increases from zero just at the surface $(y = 0)$ to the bulk value of the paste, i.e. the paste density, at some distance from the surface. In Fig. 4.18 the local paste density is shown as a function of the distance from the aggregate surface for three cements, viz. a fine, a moderate and a coarse cement. For a cement of moderate fineness Fig. 4.19 shows measured and calculated thickness and porosity of this zone. In order to enable comparison of the measured and calculated porosity the quantity is presented dimensionless.

After 1 day hydration the measured and calculated interfacial porosity are in good agreement with each other. At later ages the measured porosity is much less than the calculated porosity, particularly in the close vicinity of the aggregate surface. This discrepancy must be ascribed to the fact that in the calculated porosity only stereology- oriented effects are considered. In an actual paste, however, not only stereological aspects, but also chemistry-related aspects, i.c. densification of the matrix due to precipitation of calcium hydroxide in the water rich interfacial zone, affects the porosity in this zone.

50
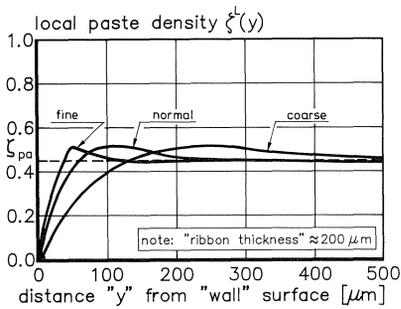
Fig. 4.18 Effect of cement fineness on the local paste density in the matrix-aggregate interfacial zone [4].
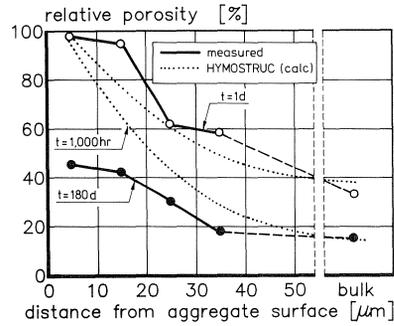
Fig. 4.19 Porosity in the matrix-aggregate interfacial zone. Experimental: after Scrivener [93]. Calculation: HYMOSTRUC [4].

5 Predictability and Practical Application

5.1 *General*

In Chapter 4 the potential of HYMOSTRUC to simulate the development of the hydration process as a function of different influencing factors as well as microstructural phenomena has been elucidated. In this chapter the predictive potential of HYMOSTRUC, i.e. the potential to predict hydration curves accurately with the default values for the model parameter $K_0(\cdot)$, $\delta_{tr}(\cdot)$, β_1 and β_2, will be dealt with. The applicability of the model for practical engineering purposes will be illustrated with the presentation of a case-study.

5.2 *Predictive Potential of HYMOSTRUC*

A real prediction of an hydration curve, i.e. a simulation with the *default values* for the model parameters $K_0(C_3S)$, $\delta_{tr}(C_2S)$, β_1 and β_2 as defined in Section 3.4.3, is shown in Fig. 5.1. In the figure two adiabatic temperature curves are presented for mixes with $\omega_0 = 0.4$ and $\omega_0 = 0.5$, respectively. The calculated curves are indicated with solid lines. For the mix with $\omega_0 = 0.5$ dashed lines indicate the predictions with 5% upper and lower bound values of $K_0(C_3S)$ and values for the transition thickness $\delta_{tr}(C_2S)$ 0.5 μm lower and higher than its default values (curves d and c). It can be concluded that the measured adiabatic temperature curves fall within the range bordered by the dashed curves calculated with the upper and lower bound values of the model parameters.

5.3 *Application of HYMOSTRUC for Practical Engineering Purposes*

5.3.1 Temperature Predictions in Concrete Structures

As indicated in the Chapter 1 HYMOSTRUC would enable us to generate adiabatic hydra-

51

temperature [°C]

d(ω₀=0.5) b(ω₀=0.5)

a(ω₀=0.4)
c(ω₀=0.5)

C₃S	C₂S	C₃A	C₄AF
63.7%	12.8%	8.4%	8.8%

Blaine = 400 m²/kg

	K_0	δ_{tr}	β_1	β_2
	μm/hr	μm	--	--
a	0.047	3.7	2	2
b	0.047	3.7	2	2
c	0.034	3.2	2	2
d	0.060	4.2	2	2

sample data:
cement: 226 kg/m³
air   : 25 l/m³
wcr   : variable
mass   : 7.849 g
ad.cal.meter: =10.4kJ/°C

time [hrs]
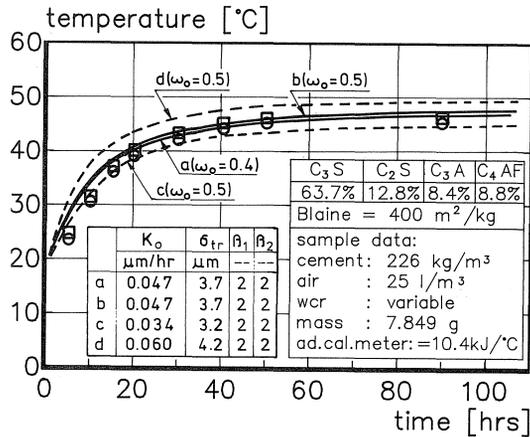
Fig. 5.1 Measured (discrete points) and predicted (solid and dashed curves) adiabatic hydration curves [4, 94].

tion curves which could serve as input for macro-level computer programs currently in use for analysis of temperature fields in actual concrete structures.

Examples of predicted adiabatic input curves and temperature calculations in hardening concrete walls carried out on the basis of these input curves are given in Fig. 5.2. Mix data is given in the inset of Fig. 5.2a. The adiabatic input curves were determined for three K_0-values, viz. the mean value according to the K_0-C_3S relationship according to equation (3.33), as well as for values corresponding to this mean value minus and plus a standard deviation $s(K_0) = 0.009$ μm/h, respectively. Transition thicknesses were chosen so as to simulate – for the cement composition is view –, a more rapid, a moderate and a more slow cement. Fig. 5.2b shows the temperatures in the core of a 1 meter thick concrete wall. Temperature calculations were carried out with TEMPSPAN, a com-

degree of hydration α

cement: 300 kg/m³
wcr: 0.5
aggregate: 1955 kg/m³
air content: 1.0 %
initial mix temp.: 15 °C
C₃S-content: 63 %
max.pot.heat: 470 kJ/kg

model parameters				
curve	K_0 μm/hr	δ_{tr} μm	β_1 –	β_2 –
I	0.055	3.5	2	2
II	0.046	3.0	2	2
III	0.037	2.5	2	2

time [hrs]

a. Adiabatic hydration curves

concrete temperature [°C]

T (ad I)
T (ad II)
T (ad III)

outside temperature
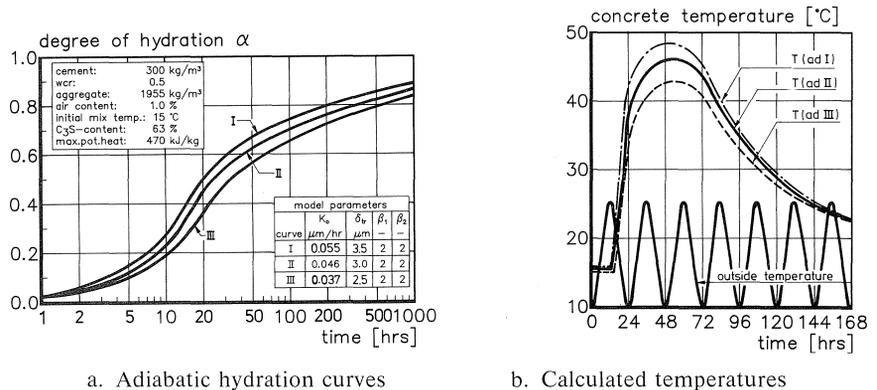
time [hrs]

b. Calculated temperatures

Fig. 5.2 a. Adiabatic hydration curves illustrating the effect of scatter in the independent model parameters on the shape of the curves.
b. Temperatures in the centre of a 1 meter thick hardening concrete wall for different adiabatic input curves.

52

puter code which calculates the progress of the hydration process, i.e. the degree of hydration, and the associated temperatures in hardening concrete structures for a given adiabatic input curve. It appears that the consequences of the relatively large scatter in the K_0- and δ_{tr}-values results in maximum temperatures from 43 °C for the slow cement to 48 °C for the rapid cement.

5.3.2 Probability of Early-Age Thermal Cracking

With TEMPSPAN the development of strength and early-age thermal stresses can be determined as a function of time. The strength is determined as a function of the degree of hydration. The stress calculations include the effect of early-age relaxation according to the procedures outlined in [89]. Results of strength and stress calculations are presented in Fig. 5.3a.

Strength and stresses being known, the theoretical probability of cracking can be determined, provided that both the distribution functions and standard deviations of the strength and stresses are known. The procedure is shown schematically in Fig. 5.3b. Both tensile strength and thermal stresses are assumed to exhibit a normal distribution. The standard deviation of the predicted stresses is assumed to be twenty percent higher than that of the tensile strength.
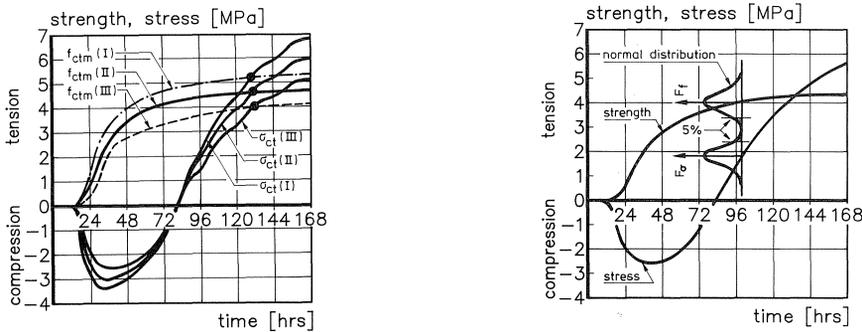
a. Tensile strength and thermal stresses   b. Probability of cracking – schematic

Fig. 5.3   a. Theoretical tensile strength and thermal stresses calculated on the basis of three adiabatic input curves.
       b. Schematic presentation of calculations for the risk of early-age thermal cracking.

The calculated probability of cracking is shown in Fig. 5.4. The calculations refer to a 0.5 m and a 1.0 m thick concrete wall and are carried out for the three adiabatic input curves given in Fig. 5.2a. It appears that the effect of the wall thickness on the risk of cracking dominates the effect of uncertainties in the input curves, i.e. in the scatter of the independent model parameters for which the adiabatic input curves had been calculated.
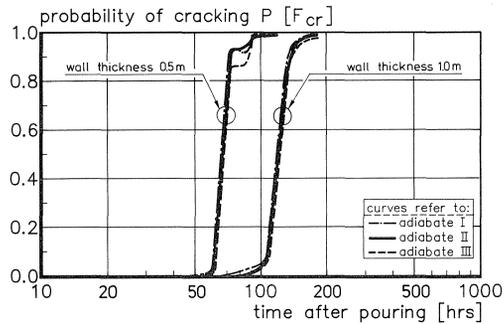
Fig. 5.4 Predicted probability of thermal cracking in two hardening concrete walls for the input curves presented in Fig. 5.2a.

From a parametric sensitivity study it could further be concluded that the effect of uncertainties in the adiabatic input curves on the calculated probability of cracking are subordinate to the effect of uncertainties in the modelling of early-age rheological behaviour, c.q. early-age plastic deformations and early-age relaxation. This result greatly enhances the applicability of HYMOSTRUC for executing sensitivity studies concerning the effect of changes in either the mix composition or pouring sequences, insulating schemes, cooling or heating of the concrete and stripping times. It also tells us that further research is required regarding the early-age rheological behaviour of cement-based materials.

6 Discussion, Conclusions and Closure

6.1 *General Remarks*

When discussing microstructural characteristics of hardened cement-based materials Wittmann [5] has stated that, because of the actual complexity of the microstructure, there is no hope that we will ever be capable of modelling the microstructure of hardened cement realistically. If this statement holds for *hardened* cement paste, it certainly holds for *hardening* pastes. Six year later, in 1986, Diamond [95], discussing the work of Jennings on microstructural development in a C_3S paste, concluded in a similar way when stating: "While the concept (of Jennings) and some of the specifics of such modelling of microstructural development can be extended to Portland cement paste, such extension is extremely difficult because of the much greater complexity of the cement system, and success should not be expected in the near future".
Against the background of these statements it is obvious that the simulation model discussed in this report, viz. HYMOSTRUC, can not be more than an *attempt*, a *step* in a certain direction. On the other hand we are convinced that the potentialities of computer-based models for simulation of complex and mutually interrelated processes and mechanisms involved in hydration and microstructural development can hardly be overestimated. In this respect it must be born in mind that with the modern generation

54

of computers huge files of information from the fields of chemistry, physics, stereology, thermodynamics, etc. become accessible and operational, thus bridging gaps between different disciplines involved and even the gap between micro- and meso-level on the one hand and the macro- or engineering level on the other hand. Bridging of these gaps is certainly to be considered one of major challenges of Computational Materials Science.

The step-wise calculation procedure, according to which HYMOSTRUC operates, makes it possible to consider a large number of non-linear phenomena and mechanisms from which we would have to refrain if we would stick to a purely analytical "closed solution" approach. The open structure of the model makes it most flexible and therefore also most attractive for both research and practical applications.

6.2 *Summarizing Remarks*

An evaluation of the results of numerical simulations conducted so far has revealed, c.q. confirmed, that:

- The formation of interparticle contacts, i.e. microstructural development, does affect the rate of hydration of individual particles quite substantially. *Hydration and micro-structural development should, therefore, be considered (and modelled) as mutually interrelated phenomena.* Ignoring microstructural development as a factor in hydration kinetics may give rise to misinterpretations as regards experimental hydration data.

- The particle size distribution of the cement is an important factor in both hydration kinetics and microstructural development (see also [4]).

- The amount of cement which is, according to the simulation model, involved in the development of interparticle contacts and which is considered a measure for the number of interparticle contacts, appears to exhibit a good correlation with the strength development. It could be verified that those particle fractions which play a major role in the formation of interparticle contacts are just those of which it is known from experimental work that they are most advantageous in view of the development of strength [4]. The observed correlation between the amount of cement involved in the development of interparticle contacts and strength seems to confirm the reasonableness of ideas put forward by, among others, Collepardi [96], Lawrence et al. [40], Granju et al. [97], Liu Chong Xi [98] and, last but not least, Rehbinder [99]. Note: The question whether chemical of physical bonds are involved here has not been addressed in the present study.

- Having modelled the effects on the rate of hydration of the *particle size distribution,* the *w/c ratio* and the *reaction temperature,* the effect of the chemical composition of the (Portland) cement could be described with mainly *two* model parameters, viz. the basic rate factor $K_0(C_3S)$, which could be written as a function of the C_3S content, and the transition thickness $\delta_{tr}(C_2S)$, which appeared to be weakly correlated to the C_2S content.

- The majority of isothermal and adiabatic hydration data analyzed so far has revealed that 28-day hydration values of Portland cement-based systems could be predicted with an accuracy of $\pm$ 5...10%. A higher accuracy is not expected to be possible unless the effects of gypsum content and minor constituents are modelled explicitly.
- The accuracy of predicted (adiabatic) hydration curves appeared to be sufficient so as to use these curves as input data for temperature and strength calculations and stress analysis in hardening concrete structures. The predicted moment of cracking turned out not to be strongly correlated to the shape of the input curves, i.e. not strongly affected by small variations in the model parameters $K_0(C_3S)$ and $\delta_{tr}(C_2S)$. The effect of the factors β_1 and β_2 on the course of the predicted hydration curves was even less significant.

Although promising results have been obtained already, it is emphasized that the model is still in its early stage of development. Further research is planned as regards the difference between paste hydration and hydration in actual concretes, modelling of hydration of non-Portland cements, the effect of additives and extra fines and the effect of pressure on both hydration and microstructural development. More chemistry-oriented information should also be inserted in the model. Particularly in case of concretes manufactured with a low w/c ratio the pore water chemistry is expected to become of increasing importance.

7   Summary

In this report, which is based on the PhD-Thesis "Simulation of hydration and formation of structure in hardening cement-based materials" [4], the potential for the use of computers for the simulation of the processes and mechanisms occurring in hardening cement-based materials is outlined. The major aim of the project was:

> "... to make well-established research results and experimental data in the various fields of study, such as *cement chemistry, physics* and *stereology,* accessible and operational for practical engineering purposes, viz. for the *prediction of adiabatic (and isothermal) hydration curves.* These curves form an essential part of the input for computer programs used for macro-level analyses of hardening concrete structures".

This research aim has been elucidated in more detail in Chapter 1 of the report. The multi-disciplinary character of the subject is outlined in Chapter 2. In that chapter, in a bird's eye view, a survey is given as aspects involved in hydration and microstructural development. Due attention has been given to the relevance of interactions between individual processes and mechanisms insofar as they might be of importance for mathematical modelling. It was concluded that none of the models for hydration processes in cement-based materials proposed so far accounted for the simultaneous formation of microstructure and the effect this might have on the rate of hydration.

A second important fact in view of mathematical modelling was that the slope of hydration curves turned out to be significantly influenced by the particle size distribution of

the cement. With regard to the chemistry-related aspect of the hydration process, it had to be concluded that the important questions as to whether hydration of individual compounds of a poly-mineral cement proceeds independently or at equal fractional rates and whether hydration products are formed topochemically or through solution have not yet been answered satisfactorily.

The main structure of a computer-based simulation model, called HYMOSTRUC (the acronym for HYDration, MOrphology and STRUCtural development), has been outlined in Chapter 3 of the report. The effects of the particle size distribution, the state of water and the reaction temperature on the rate of hydration are modelled explicitly. Based on a homogeneous distribution of the cement particles in the cement-water system and assuming a constant, albeit temperature-dependent, ratio between the volume of the reaction products and the anhydrous cement, an algorithm was developed with which the amount of cement involved in the formation of interparticle contacts can be determined. The effect of the formation of interparticle contacts on the rate of hydration of the particles involved in the interaction process has been modelled explicitly. The rate at which a concentric reaction front penetrates into a hydrating cement grain is described using a Basic Rate Equation. This rate equation comprises, besides factors which allow for the previously mentioned effects of the state of water, the formation of interparticle contacts and reaction temperature, four so-called *independent model parameters*. One of these parameters, the Basic Rate Factor $K_0(\cdot)$ [μm/h], describes the *initial* rate at which a concentric reaction front penetrates into a particular cement grain. The second model parameter has been denoted the Transition Thickness $\delta_{tr}(\cdot)$ [μm], viz. the thickness of the product layer at which the reaction changes from a boundary reaction into a diffusion-controlled reaction. The second two independent model parameters also occur in the diffusion-controlled stage. One of these factors, β_1, determines the development (linear, parabolic, cubic) of the diffusion-controlled process at the particle level. The second one, β_2, refers to the effect of temperature-related morphological changes of the reaction products on the rate of penetration.

These four model parameters have been determined in an extensive evaluation program, in which more than 60 hydration tests comprising 27 different cements were involved. In this evaluation program a distinct correlation was established between the basic rate factor K_0 and the C_3S content of the cement. The transition thickness δ_{tr} turned out to be weakly correlated with the C_2S content. No correlation could be established between the values of the coefficients β_1 and β_2 and the chemical composition of the cement. For the range in which the values of these two coefficients varied, they hardly affected the correlation between the K_0- and δ_{tr}-values and the cement composition, which substantially enhanced the reliability and applicability of the model.

The potential of the model to simulate hydration and microstructural features is discussed in Chapter 4. The amount of cement involved in the formation of interparticle contacts was assumed to be a measure of the number of interparticle bonds per unit of paste volume and, as such, a possible strength parameter. A distinct correlation between the amount of cement (per unit volume of paste) involved in the interaction mechanism and the development of strength could also be established, which seems to confirm the validity of the previous assumptions.

Explicit allowance for the stereological aspect enabled investigation into the effect of the packing of particles in the matrix-aggregate interfacial zone on the interface properties. Results of calculated widths of the matrix-aggregate interfacial zones and porosity calculations are presented.

The potential of HYMOSTRUC to predict adiabatic hydration curves as a function of the particle size distribution of the cement, the w/c ratio, the (initial) curing temperature and the chemical composition of the cement (Portland cement), and thus to serve practical engineering purposes, is evaluated in Chapter 5 in a case study.

Conclusions as regards the potentialities of the simulation model for practical and research purposes are presented in Chapter 6.

8   Notations and Symbols

A	accumulated centre-plane area (per g cement)	$[\mu m^2]$
A_{por}	total pore wall area	$[\mu m^2]$
A_{wat}	pore wall area in contact with (bulk) pore water	$[\mu m^2]$
E	(apparent) activation energy	$[kJ/mol]$
a_x	centre-plane area of particle x	$[\mu m^2]$
C_w	water concentration factor	$[-]$
d	thickness of spherical (outer) product layer	$[\mu m]$
F	particle fraction	
$F_i(\cdot)$	temperature functions (index 1 or 2)	
f	strength	$[MPa]$
$G(x)$	cumulative mass distribution of poly-size cement powder	$[g]$
I_x	cell (with central particle x)	$[\mu m^3]$
$K_0(\cdot)$	basic rate factor (phase-boundary reaction)	$[\mu m/h]$
$K_1(\cdot)$	rate constant (diffusion reaction)	$[\mu m^2/h]$
L	centre-to-centre particle distance	$[\mu m]$
N	number of particles per gram cement	
Q	heat of hydration	$[J/g]$
Q^{max}	maximum heat of hydration at complete hydration	$[J/g]$
R	universal gas constant	$[J/{}^\circ K \cdot mol]$
$R_{...}$	outer radius of expanding particles	$[\mu m]$
RH	relative humidity	
r_0	radius of anhydrous particle	$[\mu m]$
S_x	rib size of cubic cell I_x	$[\mu m]$
s	standard deviation	
T	temperature	$[{}^\circ C]$
t	time	$[h \text{ or } sec]$
V_x	volume of particle fraction F_x	$[\mu m^3]$
$V_{...}$	pore volume (capillary, total)	$[cm^3/cm^3]$
V_w	initial water volume in paste	$[cm^3/cm^3]$
v_x	volume of particle with diameter x	$[\mu m^3]$

w	amount of water	[g]
x	particle diameter (also used as particle counter)	[μm]
$\alpha(t)$	degree of hydration at time t	[−]
β_i	independent model parameters (index 1 or 2)	
β_{RH}	reduction factor, accounting for relative humidity effects	
Γ	thickness of adsorption layer	[μm] or [Å]
δ	thickness of layer of reaction products	[μm]
ζ	volumetric density factor	[μm³/μm³]
λ	parameter, indicating the type of reaction process (Section 3.4.2)	
ν	ratio: volume of hydration products/reactant	[−]
ϱ	specific mass	[g/cm³]
σ	stress	[MPa]
ϕ	pore diameter	[μm] or [Å]
χ	stereometric conversion factor $(= (4 \cdot \pi/3)^{1/3})$	[−]
$\Omega_1(x, \alpha_j)$	reduction or partition factor (water withdrawal mechanism)	[−]
$\Omega_2(\alpha_j)$	reduction factor, allowing for distribution of water	[−]
$\Omega_3(\alpha_j)$	reduction factor, allowing for amount of water	[−]
ω_0	water/cement ratio	[−]

Indices
Superscripts

| c | cubic |
| L | local |

Subscripts

ad	adsorbed (water at pore walls)
c	concrete
cap	capillary (in V_{cap})
ce	cement
ct	strength index: tension
ctk	concrete tensile strength index, characteristic value
ctm	concrete tensile strength index, mean value
em	embedded (– cement volume, – centre plane area)
fr	free (– particles; i.e. not embedded particles; – water)
in	inner (– product, – shell)
in	penetration depth of reaction front (in: δ_{in})
j	time index, indicating subsequent time steps
ou	outer (– product, – shell)
pa	paste
por	pores (in V_{por})
sh	shell
tr	transition (in: δ_{tr})
w	water
x	particle with diameter x [μm]

59

9 Abbreviations

ACI(-J)	American Concrete Institute (Journal of -)
ACR	Advances in Concrete Research
ASTM	American Society of Testing Materials
CCR	Cement and Concrete Research (Journal)
CEA	Concrete at Early Ages (RILEM Symposium)
DAfST	Deutscher Ausschuss für Stahlbeton
IC(S)CC	International Congress (Symposium) on the Chemistry of Cements
JACS	Journal of the American Ceramic Society
JCIS	Journal of Colloidal and Interface Science
M&C	Materiaux et Construction
MCR	Magazine of Concrete Research
PCCRPC	Proceedings of Chemistry and Chemistry-Related Properties of Cement
RMCTP	Revue des Materiaux de Construction et de Travaux Public
SMDDHC	Symposium on Microstructural Development During Hydration of Cement
SP	Special Publication
SR	Special Report
SSPCPC	Symposium on Structure of Portland Cement Paste and Concrete
TIZ	Tonindustrie Zeitung
ZKG	Zement, Kalk, Gips

10 References

1. BAZANT, Z. P. (1988), CCR, Vol. 18, No. 6, pp. 923–932.
2. VONK, R. A. et al. (1988), Cement, No. 7/8, pp. 53–57.
3. MAYERS, A. H. (1990), Camber Development in Prestressed Girders, Delft, 1990, (in Dutch).
4. BREUGEL, K. VAN (1991), Simulation of hydration and formation of structure in hardening cement-based material, PhD, Delft, 295 p.
5. WITTMANN, F. H. (1980), 7th ICCC, Paris, Vol. I, Sub-theme VI-2, pp. VI-2/1-14.
6. JENNINGS, H. M. (1986), SMDDHC, Boston, MRS, Proc. Vol. 85, pp. 291–300.
7. ANDEREGG, F. O., et al. (1929), Proc. ASTM, 29. Ibid. Venaut, M., [52].
8. MICHAELIS, W. (1909), Chem. Zeitung, 5, p. 9.
9. KITTL, P. et al. (1980), 7th ICCC, Paris, 1980, Vol. II, pp. II-7-11.
10. LE CHATELIER, H. (1905), McGraw Publ. Co. New York.
11. SHEBL, F. A. et al. (1985), CCR, 15, pp. 747–757.
12. DAIMON, M. et al. (1971), CCR, Vol. 1, No. 4, pp. 391–401.
13. TAPLIN, J. H. (1959), Aust. J. Appl. Sci., 10, pp. 329–345.
14. LEA, F. M. (1970), The Chemistry of Cement and Concrete, 3rd. ed., Edward Arnold Ltd.
15. MENETRIER, D. et al. (1980), CCR, Vol. 10, No. 3, pp. 425–432.
16. RUMYANTSEV, P. F. (1980), 7th ICCC, Paris, Vol. III, pp. VI-79-82.
17. TSUMURA, S. (1966), ZKG, Jhg. 19, No. 11, pp. 511–518.
18. BROWNMILLER, L. T. (1943), ACI-J, Vol. 14, No. 3, pp. 193–210.
19. REXFORD (1943), ACI-J, Vol. 14, No. 6, pp. 212/1-3.
20. BENTUR, A. et al. (1979), JACS, Vol. 62, No. 7-8, pp. 362–366.
21. YAMAGUCHI, G. et al. (1960), ZKG, No. 10, pp. 467–478.
22. LEHMANN, H. et al. (1965), TIZ, No. 15/16, pp. 337–350.
23. KEIL, F. (1971), Zement, Springer Verlag, 1971, 439 p. (in German). Ibid. Powers [24].

24. Powers, T. C. et al. (1946/1947), ACI-J, Part 1–9.
25. Czernin, W. (1954), ZKG, Jhg. 7, No. 12, pp. 460–464.
26. Setzer, M. J., DAfSB, Heft 280, Wilhelm Ernst & Sohn. KG., pp. 43–117.
27. Sabri, S. et al. (1980), 7th ICCC, Paris, Vol. III, pp. VI-52–55.
28. Locher, F. W. et al. (1976), ZKG, Jhg. 29, No. 10, pp. 435–442.
29. Schwiete, H. E. et al. (1966), SSPCPC, ACI-SR-90, pp. 353–367.
30. Grudemo, A., The Cryst. Struct. of Cem. Hydr. – A New Gel Structure Model; pp. 62.
31. Young, J. F. et al., Doc. prepared by RILEM TC69, 27 p.
32. Copeland, L. E. et al. (1962), Disc. on Ref. 4 in 4th ISCC, Wash., pp. 648–655. Ibid. [100].
33. Wischers, G. et al. (1982), Beton, No. 9, pp. 337–341; No. 10, 1982, pp. 379–386.
34. Richartz, W. et al. (1965), ZKG, Jhg. 18, No. 9, pp. 449–459.
35. Budnikov, P. P. et al. (1966), ACI-SP 90, Washington, pp. 431–446.
36. Ciach, T. D. et al. (1971), CCR, 1, 2, p. 143; p. 159; 3, p. 257; 4, p. 367; 5, p. 515.
37. Dagleish, B. J. et al. (1980), CCR, Vol. 10, No. 5, pp. 665–676.
38. Granju, J. L. et al. (1984), CCR, Vol. 14, No. 2, pp. 249–256, No. 3, pp. 303–310.
39. Diamond, S. (1986), 8th ICCC, Rio de Jan., Vol. I, pp. 122–147.
40. Lawrence, F. V., et al. (1973), CCR, 3, No. 2, pp. 149–161; 4, No. 3, 1974, pp. 481–483.
41. Daimon, M. (1980), 7th ICCC, Paris, Vol. II, Theme III-2/1–9.
42. Scrivener, K. L. (1986), 8th ICCC, Rio de Jan., Vol. II, pp. 389–393.
43. Kühl, H. (1930), Zement, Jhg. 19, pp. 604–608; Jhg. 20, p. 196. Ibid. Gründer, W., 1950, ZKG.
44. Odler, I. et al. (1986), SMDDHC, Mat. Res. Soc., Boston, 1986, Proc. Vol. 85, pp. 33–38.
45. Kjellsen, K. O. et al. (1990), CCR, Vol. 20, No. 2, pp. 308–311.
46. Verbeck, G. J. et al. (1968), 5th ISCC, Tokyo.
47. Kjellsen, K. O. et al. (1990), CCR, Vol. 20, No. 6, pp. 927–933.
48. Kjellsen, K. O. et al. (1991), CCR, Vol. 21, No. 1, pp. 179–189.
49. Popovics, S. (1980), 7th ICCC, Paris, Vol. III, pp. VI-47–51.
50. Parrott, L. J. et al. (1990), CCR, Vol. 20, No. 6, pp. 919–926.
51. Glasstone, S. et al. (1941), The Theory of Rate Processes, McGraw Hill Book Comp., NY.
52. Venaut, M. (1961), Rev. M&C, 549, pp. 333–351; 552, pp. 393–406; 552, pp. 434–443.
53. Hakvoort, G. (1978), Formation and dissolution of AgMO2 compounds, PhD, Delft, p. 212.
54. Kondo, R. et al. (1968), 5th ICCC, Tokyo, Vol. II, Sess. II-4, pp. 203–248.
55. Taplin, J. H. (1968), 5th ICCC, Tokyo, paper II-70, pp. 337–348.
56. Bezjak, A. et al. (1980), CCR, Vol. 10, No. 4, pp. 553–563.
57. Knudsen, T. (1984), CCR, Vol. 14, No. 5, pp. 622–630.
58. Pommersheim, J. M. et al. (1980), 7th ICCC, Paris, Theme VI, pp. 195–200.
59. Pommersheim, J. M. et al. (1982), CCR, Vol. 12, No. 6, pp. 765–772.
60. Parrott, L. J. et al. (1984), PCCRPC, Ed. D. Glasser.
61. Knudsen, T. (1980), 7th ICCC, Paris, 1980, Vol. II, pp. I-170–175.
62. Bezjak, A. (1983), CCR, Vol. 13, No. 2, pp. 186–196.
63. Bezjak, A. (1983), CCR, Vol. 13, No. 3, pp. 305–318.
64. Pommersheim, J. M. (1986), SMDDHC, Boston, MRS, Proc. Vol. 85, pp. 301–306.
65. Pommersheim, J. M. et al. (1986), CCR, Vol. 12, pp. 440–450.
66. Röhling, S. et al., Kinetic Model of Structural Formation and Strength Development, Priv. Communication.
67. Frohnsdorff, G. J. C. et al. (1968), 5th ICCC, Tokyo, Vol. II, pp. 321–327.
68. Garboczi, E. J. (1992), 9th ICCC, New Delhi, November (to be published).
69. Bentz, D. P. et al. (1991), CCR, Vol. 21, pp. 325–344.
70. Stroeven, P. (1973), Some Aspects of the Micromechanics of Concrete, PhD, Delft, 329 p.
71. Wittmann, F. H. (1982), RILEM Symp. CEA, Paris, Vol II, Sess. VI, pp. 187–201.
72. Alujevic, V. et al. (1986), CCR, Vol. 16, No. 5, pp. 695–699.
73. Hagymassy, J. et al. (1969), JCIS, Vol. 29, No. 3, pp. 485–491.
74. Fraay, A. L. A. (1980), Fly Ash a Pozzolan in Concrete, PhD, Delft.
75. Jonassen, J.-E. (1982), RILEM, Int. Conf. CEA, Paris, 1982, Vol. II, pp. 213–218.
76. Rastrup, E. (1954), MCR, September, pp. 79–90.
77. Schlüssler, K. H. (1986), CCR, Vol. 16, pp. 215–226.

78. ODLER, I. et al. (1989), CCR, Vol. 19, No. 2, 1989, pp. 295–305.
79. JAMBOR, J. (1963), MCR, Vol. 15, No. 45, pp. 131–142.
80. BEZJAK, A. et al. (1980), 7th ICCC, Paris, Vol. II, pp. 111–116.
81. KROGBEUMKER, G. et al. (1972), ZKG, Jhg. 25, No. 9, 1972, pp. 417–418.
82. LHOPITALLIER, P. et al. (1948), XXI Congr. Chem. Ind., Bruxelles. Ibid. Venaut, M., [52].
83. STEINHERZ, A. R. (1960), RMCTP, No. 536. Ibid. Venaut, M., [52].
84. KEIENBURG, R. R. (1976), Particle Size Distribution and Norm Strength of PC, PhD, Karls-ruhe, 111 p. (in German).
85. DANIELSSON, U. (1960), 4th. ISCC, Washington, Vol. I, pp. 519–526.
86. LERCH, W. et al. (1948), ACI-J, Vol. 44, pp. 745–795.
87. LAUBE, M. (1990), Constitutive Model for Calculation of Thermal Stresses in Mass Concrete, PhD, 251 p., (in German).
88. RAKEL, K. (1965), Beitrag zur Bestimmung der Hydratationswärme von Zem., PhD, Aachen, 149 p.
89. BREUGEL, K. VAN (1980), Artificial Cooling of Hardening Concrete, Delft, Res. Rep. 5–80–9.
90. LOCHER, F. W. (1976), Beton, H. 7, pp. 247–249; No. 8, pp. 283–285.
91. POWERS, T. C., Ibid. Locher, F.W. [90].
92. FAGERLUND, G. (1987), Seminar on Hydration of Cement, Copenhagen, 56 p.
93. SCRIVENER, K. L. et al. (1988), ACR, Vol. I, No. 4, pp. 230–237.
94. ENCI, 1986, Adiabatic Temperature rise at different w/c ratios. Privat documentation.
95. DIAMOND, S. (1986), SMDDHC, Boston, Mat. Res. Soc., Proc. Vol. 85, pp. 21–31.
96. COLLEPARDI, M. (1972), CCR, Vol. 2, No. 1, pp. 57–65; Vol. 2, No. 5, pp. 633–636.
97. GRANJU, J. L. et al. (1980), CCR, Vol. 10, No. 5, pp. 611–621.
98. LIU CHONG XI (1987), ZKG, Jhg. 40, No. 2, pp. 103–108.
99. REHBINDER, P. A., Ibid. Jambor, J., [79].
100. KROKOSKY, E. M. (1970), M&C, Vol. 3, No. 17, pp. 313–323.